

# Breast Tumor Classification Based on Decision Information

## Genes and Inverse Projection Sparse Representation

Xiaohui Yang<sup>1</sup>, Wenming Wu<sup>1</sup>, Yunmei Chen<sup>2</sup>, Xianqi Li<sup>2</sup>,  
Juan Zhang<sup>3</sup>, Dan Long<sup>3</sup>, Lijun Yang<sup>1</sup>

1. Data Analysis Technology Lab, Institute of Applied Mathematics, Henan University,  
Kaifeng 475004, China
2. Department of Mathematics, University of Florida, Gainesville
3. Zhejiang Cancer Hospital, Hangzhou 310022, China

**Abstract:** Microarray gene expression data-based breast tumor classification is an active and challenging issue. In this paper, a robust breast tumor recognition framework is presented based on considering reducing clinical misdiagnosis rate and exploiting available information in existing samples. A wrapper gene selection method is established from a new perspective of reducing clinical misdiagnosis rate. The further feature selection of information genes is fulfilled by a modified NMF model, which is motivated by hierarchical learning and layer-wise pre-training strategy in deep learning. For completing the classification, an inverse projection sparse representation (IPSR) model is constructed to exploit information embedded in existing samples, especially in test ones. Moreover, the IPSR model is optimized via generalized ADMM and the corresponding convergence is analyzed. Extensive experiments on three public breast tumor datasets show that the proposed method is stable and effective for breast tumor classification. Compared to the latest literature, there is 14% higher in classification accuracy. Specificity and sensitivity achieve 94.17% and 97.5%.

**Keywords:** Breast tumor classification, decision information genes, layer-wise pre-training sparse NMF, inverse projection sparse representation, generalized ADMM

### 1. Introduction

Breast tumor has become the most common malignant neoplasm for women. 37.3% of breast tumor can be cured, especially in the case of early detection [1]. Effective breast tumor classification plays an important role in clinical diagnosis and treatment.

Microarray technology with its ability to simultaneously interrogate 10,000–40,000 genes has changed people’s thinking of molecular classification of human tumors [24]. It’s necessary to effectively explore and analyze breast tumor pathogenesis from the molecular biology aspects [54] [55] [56]. However, microarray gene expression data have the characteristics of small samples (patients), high dimensions (thousands of genes) and high redundancy [2], which impose a challenge to breast tumor classification. It is well known that gene representation and classifier design are critical, active and challenging issues for breast tumor classification.

Gene selection aims to remove irrelevant and redundant genes and obtain small set of information genes. There are three general approaches for gene selection: filters [50, 51], embedded methods [53] and wrappers. As a filter type method, BW [50] has the characteristics of simplicity and stability. T. Chen et.al [57] proposed a neighborhood rough sets and entropy-based filter gene selection method. Dashtbanet.al [60] proposed an evolutionary technique-based filter gene selection method. However, filter methods can’t guarantee the classification effect because they ignore the relationship between gene selection and late classification. Algamal et.al [59] proposed a sparse logistic regression-based embedded gene selection method for high-dimensional microarray data. However, embedded gene selection methods combined gene selection and classification in an optimization process, where classifier training may weaken the ability of gene selection to a certain extent. Moreover, the process and computationally are complex, there are certain requirements on the hardware conditions. It is interesting to propose a simple and adaptive gene selection method based on clinical diagnosis and classification.

Based on gene selection, feature selection aims to obtain better gene representation and further improve late classification effect. In recent years, non-negative matrix factorization (NMF) [26] and its improved methods[8] [9] [10] based feature selection for microarray gene expression data have achieved good results [47] [61] [62] [58]. Deep learning is an popular feature representation learning method [36] and has achieved preliminary results in breast tumor classification recognizing benign and malignant breast cancer [30]. However, the success of deep learning needs to be built

on the premise of large-scale training data, complex network structures, high-performance GPU devices and optimized parallel algorithms. Deep learning for little data is still an open problem. Other strategies for data representation and feature extraction are well understood [17][7], topic models combine data modeling with optimization to learn interpretable and consistent features in data [21][11]. It is worthy believing that a better breast tumor classification effects can be achieved by utilizing complementary advantages of different methods. For example, NMF-based feature selection methods may be improved by integrating deep learning techniques. The literature [37] proposes to use SNMF to perform gene selection and feature extraction on gene expression data, and complete tumor classification based SVM.

Classification design is another critical issue for tumor classification. Common used classification methods for microarray gene expression data have fisher linear discriminant analysis [33], nearest neighbor (NN) [52], Random Forest (RF) [34], neural networks (NN)[35], support vector machine (SVM)[28]. Most of these methods are based on statistical theory, relying heavily on model parameters and most likely “over-fitting”. Sparse representation is a sparse coding technique based on an over-completed dictionary. Sparse representation based classification (SRC) was originally proposed by Wright et al. for face recognition [29]. Recently, SRC and its improved methods are widely used in microarray gene expression profiling based tumor classification [14, 15, 18, 20]. For tumor classification, however, it is small data problem and difficult to acquire effective labeled samples. It is worth noting that the success of SRC depends on enough training data of the same category. Zhang et al. [23] indicates that the discrimination ability of SRC will be reduced when there is a small disturbance on representation error. Our previous work [13] proposed an inverse projection-based pseudo-full-space representation classification (PFSRC) method for face recognition. PFSRC focused on exploiting complementary information between training samples and test samples by utilizing existing available samples rather constructing auxiliary training samples. For face recognition, especially the occluded faces, there are complementarities between samples, while it is not obvious for gene expression profile data.

From another viewpoint, it can be seen that sparse representation based breast tumor classification belongs to under determined linear model. To solve this problem, different constraint conditions have been added into model by considering priori information of practical problems. In the field of tumor recognition based on microarray gene expression data, sparse information is important prior information, which embodies  $l_1$ -regularization constraint for the representation model. There are many ways to optimize a  $l_1$ -regularization problem, for example liner Bregman [22], least angle regression (LARS) [44] and alternating direction method of multipliers (ADMM) [40[41]]. ADMM attracts a great deal of attention in biostatistics. It mainly deals with convex optimization problems with constraints. Xiao et al. [41] proposed a generalized ADMM with Semi-Proximal Terms, denoted as GADMM. It is also verified that the convergence error is less than classic ADMM and the convergence speed is faster than classic ADMM [41].

Motivated by these works, a robust breast tumor classification is proposed. It is noted that the work focuses on utilizing existing available samples rather than constructing auxiliary training samples. The main differences between the proposed technique and the related works [50], [43] and [13] are as follows. (1) Compared to existing gene selection methods, the proposed wrapper gene selection technique is presented based on decision information factor (DIF), which is established for the first time by utilizing decision curve analysis (DCA) [45] to distinguish the loss of clinic misdiagnosis rate brought by clinical diagnosis. We select the genes that can reduce misdiagnosis rate in breast tumor classification. (2) An improved NMF model, layer-wise pre-training multi-layer sparse NMF (LPML-SNMF), is proposed to learn features that are beneficial to breast classification. The LPML-SNMF is based on the hierarchical learning and layer-wise pre-training mechanism of deep learning. SNMF [27] is another improved NMF method, however, SNMF only considers the characteristics of data sparse and does not delve deeper into useful information contained in the features. (3) An inverse projection sparse representation classification model is presented to fully explore information embedded in existing samples,

especially test samples. The proposed model is optimized by GADMM and the corresponding convergence is analyzed.

The remainder of this paper is organized as follows. The methodology is given in section 2. In Section 2.1, DIF is established for gene selection. Section 2.2 gives LPML-SNMF based information genes feature selection. LPML-SNMF model is optimized and optimization LPML-SNMF model. In Section 2.3, IPSR model is proposed and optimized by GADMM. Extensive experiments on three public breast tumor gene expression datasets are shown in Section 3. Finally, conclusions are conducted in Section 4.

## **2. Methodology**

### **2.1 Gene selection based on decision information factor**

In this subsection, a simple and effective quantitative index named decision information factor (DIF) is established, which for the first time considers the performance of clinical misdiagnosis rate loss based on DCA. And then a DIF-based wrapper gene selection method is proposed to select genes for reducing the clinical misdiagnosis rate as much as possible.

#### **2.1.1 Construction of DIF**

Receive operating characteristic curve (ROC) is a graphical plot that illustrates the diagnostic ability of a binary classifier system as its discrimination threshold is varied [38]. However, ROC focuses on accuracy without considering misdiagnosis rate and missed diagnosis rate, while clinic demands are more concerned with the latter. For tackling this problem, (Andrewvickers, Memorial, Sloan KettCancer Institute, 2006) [45] proposed a “decision curve” to describe the relationship between net benefit against threshold probability. Similar to ROC, DCA is firstly proposed for evaluating prediction models. Motivated by the characteristics of DCA, it is well known that decision analytic methods often require explicit valuation of health states or risk-benefit ratios for a range of outcomes. A gene that helps diagnose breast tumors will have a high net benefit (NB). Therefore, for the first time, we introduce DCA into gene selection. The main idea of this lies in distinguishing the performance of clinical misdiagnosis rate loss for gene selection in breast tumor classification. The smaller

the misdiagnosis rate of loss of genes are, the better the genes are. In order to use DCA for gene selection, an indicator called DIF is defined as follows.

Decision-curve interpretation of clinical trials for gene selection: If the gene has a definite benefit for diagnosis, the gene should be used for breast tumor classification; if it is clearly ineffective, it should not be used. The higher NB gene in DCA is favorable for classification. First, a brief review of NB in DCA? The NB can be expressed as [45]

$$NB = \frac{TP}{n} - \frac{FP}{n} \times \frac{p_t}{1 - p_t}, \quad (1)$$

where  $TP$  and  $FP$  represent numbers of patients with true- positive and false-positive results.  $p_t$  is threshold probability.  $n$  is the total number of patients. In short, we subtract the proportion of all patients who are false-positive from the proportion who are true-positive, weighting by the relative harm of a false-positive and a false-negative result.

There have two extreme cases: One, assume all patients are positive (treat all). Suppose  $P$  is the number of true-positive patients. It can obtain

$$D_1 : NB = \frac{P}{n} - \frac{n - P}{n} \times \frac{p_t}{1 - p_t},$$

Two, draw a straight line parallel to the  $x$ -axis ( $p_t$ ) at  $y = 0$  representing the net benefit associated with the strategy of assuming that all patients are negative:

$$D_2 : NB = 0.$$

The intersection of  $D_1$  and  $y$ -axis is the prevalence  $p$ . The intersection of  $D_2$  and  $x$ -axis is the prevalence  $p$  too [45].

As shown in Fig.1, with the prevalence  $p$  as the critical point, the NB before  $p$  does not include all patients. We hope to find a gene that can be used to diagnose all patients, rather than consider only a part of the patients. However, in between these two extremes  $D_1$  and  $D_2$  there is a range of where the prediction model is of value

[45]. So we consider the NB in the threshold interval between prevalence  $p$  to  $D_1$  and  $D_2$ , the threshold interval  $p \leq p_t \leq 1$ . In order to use DCA for gene selection, an indicator called DIF is defined as follows.

**Definition 1 (Decision Information Factor, DIF):** suppose  $p_t$  is the threshold probability, then we have

$$DIF = \max_{p \leq p_t \leq 1} \left( \frac{TP}{n} - \frac{NP}{n} \times \frac{p_t}{1 - p_t} \right), \quad (2)$$

where  $p$  represents prevalence, It's obvious that  $DIF \in [0,1]$ .

We want to know how big a NB can be for a breast tumor diagnosis in a range of genes. The more NB brought, the more helpful the clinical diagnosis. Fig.1 shows the DIF acquisition of a gene. Therefore, we can select gene based DIF to sort the DIFs of all genes. The larger the DIF, the more helpful the classification.

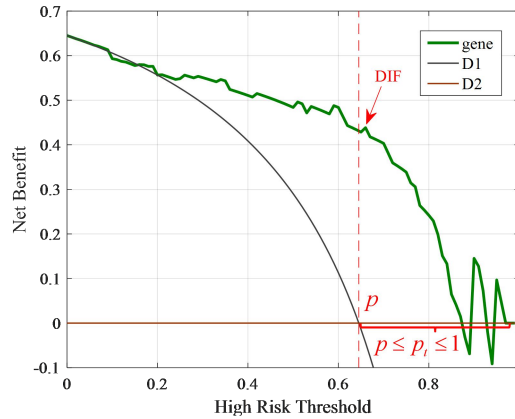


Fig.1. A DCA figure of a gene

## 2.2 Feature selection based on LPML-SNMF model

In this subsection, an improved NMF method named LPML-SNMF is proposed and used for information gene feature selection. The advantages of LPML-SNMF is that the hierarchical learning and the layer-wise pre-training strategy.

In order to dig more effectively breast tumor data in favor of classification information, selection the relevant features for breast tumor classification. The information genes obtained by DIF are feature selected by LPML-SNMF. With the idea of deep learning, the idea of layer-wise pre-optimization is added to our model, which is motivated by deep learning. Based on the hierarchical learning mechanism of

depth learning and the layer-wise pre-training strategy, an improved NMF method is proposed for feature selection of information genes. And the LPML-SNMF model is pre-trained layer by layer to further improve the breast tumor classification performance. The each layer of LPML-SNMF model is the same as the SNMF [27] model from the optimization point of view. Therefore, the same solution as SNMF is adopted, and the variables are alternately iterated by gradient descent method.

### 2.2.1 NMF

NMF is a group of algorithms in multivariate analysis and linear algebra where a matrix  $V$  is factorized into two matrices  $W$  and  $H$ , with the property that all three matrices have no negative elements [26]. Suppose  $V = [V^{training} \ V^{test}] \in R^{p \times q}$  is the information genes data set, where  $V^{training}$  and  $V^{test}$  are training set and test set, respectively. And column representative sample, row represents the gene. Mathematical model expressed as,

$$V \approx WH,$$

where  $W \in R^{p \times r}$  is called basis matrix, each column of  $H \in R^{r \times q}$  is called an encoding and is in one-to-one correspondence with  $V$ , The rank  $r$  of the factorization is generally chosen so that  $(p+q)r < pq$ . The matrix  $W, H$  are non-negative.

### 2.2.2 SNMF

Hoyer et. al. [27] proposes a SNMF, which adds sparse regularization constraints to  $H$ . Combining the goal of small reconstruction error with that of sparseness, one arrive at the following objective function to be minimized:

$$\min_{W, H} \frac{1}{2} \|V - WH\|_F^2 + \lambda_1 \sum_{i=1}^q \|h_i\|_1, s.t. \ W \geq 0, \ H \geq 0, \quad (3)$$

where  $\lambda_1$  is regularization parameter,  $H = [h_1, h_2, \dots, h_q], h_i \in H, i = 1, \dots, q$ .

The microarray gene expression profile data itself is sparse. Therefore, the model is improved on the basis of SNMF and used for gene selection.

### 2.2.2 Multi-layer SNMF



SNMF only considers prior information from sparse regular terms and does not have deeper exploration of useful information hidden in features. In order to deepen the useful information hidden in the data, we introduced the deep ideas in deep learning into the SNMF model and proposed ML-SNMF. In the following, we perform  $l$ -layer NMF decomposition of  $V$ ,

$$\begin{aligned} \min_{W_1, \dots, W_l, H_l} \quad & \frac{1}{2} \|V - W_1 W_2 \dots W_l H_l\|_F^2 + \lambda_1 \sum_{i=1}^q \|W_2 \dots W_l (h_1)_i\|_1 + \dots + \lambda_l \sum_{i=1}^q \|(h_l)_i\|_1, \\ \text{s.t.} \quad & W_1 \geq 0, \dots, W_l \geq 0, H_l \geq 0. \end{aligned} \quad (4)$$

Two-layer sparse NMF model can be written as follows,

$$\begin{aligned} \min_{W_1, W_2, H_2} \quad & \frac{1}{2} \|V - W_1 W_2 H_2\|_F^2 + \lambda_1 \sum_{i=1}^q \|W_2 (h_2)_i\|_1 + \lambda_2 \sum_{i=1}^q \|(h_2)_i\|_1, \\ \text{s.t.} \quad & W_1 \geq 0, W_2 \geq 0, H_2 \geq 0. \end{aligned} \quad (5)$$

where  $(h_2)_i \in R^{r_2 \times 1}, i=1, \dots, q$  represent the coefficient code corresponding to the  $i$ -th sample  $v_i$ ,  $H_2 = [(h_2)_1, \dots, (h_2)_q] \in R^{r_2 \times q}$ .

### 2.2.3 LPML-SNMF and its optimization

Optimization of NMF and SNMF are unstable because their results heavily dependent on the initial value of NMF decomposed. In order to alleviate this instability, hierarchical learning and layer-wise pre-training (LP) strategy is introduced, which has been indicated useful for deep learning. The corresponding improved NMF model is layer-wise pre-training multi-layer SNMF (LPML-SNMF).

The each layer of LPML-SNMF model is similar to SNMF model [27] from the optimization point of view. Therefore, the same solution as SNMF is adopted, and the variables are alternately iterated by gradient descent method.

Suppose the decomposition level is  $l$ , the SNMF model of each layer is shown as

$$\min_{W_l, H_l} \quad \frac{1}{2} \|H_{l-1} - W_l H_l\|_F^2, \quad \text{s.t.} \quad W_l \geq 0, H_l \geq 0, l=1, 2, \dots. \quad (6)$$

where  $H_0$  represent  $V$ . Combining the goal of small reconstruction error with that of sparseness, one can arrive at the following objective function to be minimized:

$$\min_{W_l, H_l} \frac{1}{2} \|H_{l-1} - W_l H_l\|_F^2 + \lambda_j \sum_{i=1}^q \|(h_l)_i\|_1 \quad s.t. \quad W_l \geq 0, \quad H_l \geq 0, \quad l=1, 2, \dots \quad (7)$$

Taking an example of two-layer, the model is shown as follows,

$$\min_{W_1, H_1} \frac{1}{2} \|V - W_1 H_1\|_F^2 + \lambda_1 \sum_{i=1}^q \|(h_1)_i\|_1 \quad s.t. \quad W_1 \geq 0, \quad H_1 \geq 0, \quad (8)$$

$$\min_{W_2, H_2} \frac{1}{2} \|H_1 - W_2 H_2\|_F^2 + \lambda_2 \sum_{i=1}^q \|(h_2)_i\|_1 \quad s.t. \quad W_2 \geq 0, \quad H_2 \geq 0. \quad (9)$$

where mixing matrix  $W_1 \in R^{p \times r_1}$ ,  $W_2 \in R^{r_1 \times r_2}$ ,  $(h_2)_i \in R^{r_2 \times 1}, i=1, \dots, q$  represent the coefficients corresponding to the  $i$ -th sample  $v_i$ ,  $H_2 = [(h_2)_1, \dots, (h_2)_q] \in R^{r_2 \times q}$ .  $r_1, r_2$  represent the matrix decomposition dimension, and  $r_1 \ll \min\{p, q\}$ ,  $r_2 \ll \min\{r_1, q\}$ . Eq. (8) and (9) are the LPML-SNMF model.

We will first consider optimizing  $H_1$ , for a given basis  $W_1$ . As the objective (8) is quadratic with respect to  $H_1$ , and the set of allowed  $H_1$  (i.e. the set where  $(H_1)_{ij} \geq 0$ ) is convex, we are guaranteed that no suboptimal local minima exist. To address these concerns, reference [27]. This is given by iterating the following update rule:

$$H_1^{k+1} = H_1^k \cdot (W_1^k)^T V \cdot ((W_1^k)^T W_1^k H_1^k + \lambda_1), \quad (10)$$

We consider optimizing the objective (13) with respect to both the basis  $W_1$  and the hidden components  $H_1$ , under the stated constraints. First, we consider the optimization of  $W_1$  only, holding  $S$  fixed.

$$W_1^{k+1} = W_1^k - \mu_1 (W_1^k H_1^{k+1} - V) (H_1^{k+1})^T, \quad (11)$$

For the constraints  $W_1, H_1 \geq 0$ . We construct the projection operators

$$\begin{aligned}\hat{h}_{1ij} &= \begin{cases} h_{1ij}, & \text{if } h_{1ij} \geq 0, \\ 0, & \text{otherwise.} \end{cases} \quad h_1 \in H_1^{k+1}, \\ \hat{w}_{1ij} &= \begin{cases} w_{1ij}, & \text{if } w_{1ij} \geq 0, \\ 0, & \text{otherwise.} \end{cases} \quad w_1 \in W_1^{k+1}.\end{aligned}\tag{12}$$

where  $\mu > 0$  is step size. This combined step consists of a gradient descent followed by projection onto the closest point satisfying both the non-negativity and the unit-norm constraints.

Similar to model (8), model (9) can be optimized as follows.

$$H_2^{k+1} = H_2^k \cdot (W_2^k)^T H_1 / ((W_2^k)^T W_2^k H_2^k + \lambda_2),\tag{13}$$

$$W_2^{k+1} = W_2^k - \mu_2 (W_2^k H_2^{k+1} - H_1) (H_2^{k+1})^T,\tag{14}$$

$$\begin{aligned}\hat{h}_{2ij} &= \begin{cases} h_{2ij}, & \text{if } h_{2ij} \geq 0, \\ 0, & \text{otherwise.} \end{cases} \quad h_2 \in H_2^{k+1}, \\ \hat{w}_{2ij} &= \begin{cases} w_{2ij}, & \text{if } w_{2ij} \geq 0, \\ 0, & \text{otherwise.} \end{cases} \quad w_2 \in W_2^{k+1}.\end{aligned}\tag{15}$$

To optimize the obtain the convergence solution of the objective function in (9),  $H_2$  and  $W_2$  can be updated in turn.

The comparison of NMF and other improved NMF methods is given in subsection 3.3. [42] [43] proposes a multi-layer NMF (ML-NMF), in order to verify our model and compare it with it.

### 2.3 IPSRC model

In this section, the methodology of the presented breast tumor classification is described. Firstly, sparse representation [29] and PFSR [13] are briefly reviewed. Then, the IPSR is proposed and optimized by GADMM. The corresponding convergence analysis is given.

#### 2.3.1 Inverse projection representation

Suppose  $X = [x_1, \dots, x_{s_1}, \dots, x_{s_c}] \in R^{d \times s_c}$  are training samples,  $x_i \in X$ ,  $i = 1, 2, \dots, s_c$  represent each training sample.  $X_j = [x_{s_{j-1}+1}, \dots, x_{s_j}] \in R^{d \times (s_j - s_{j-1})}$  are the  $j$ -th category

samples,  $j = 1, \dots, c$  is the number of category, be  $s_c$  labeled training samples in total of  $c$  categories. Similarly, suppose  $Y = [y_1, \dots, y_k] \in R^{d \times k}$  are test samples,  $k$  expresses the number of test samples.  $y_l \in Y$ ,  $l = 1, 2, \dots, k$  represent each test sample.

Sparse representation [29] assumes that each test sample  $y_l \in R^d$ , can be linearly represented by sufficient training samples from the same category,

$$y_l = \gamma_{l,1}x_1 + \dots + \gamma_{l,s_c}x_{s_c} = \sum_{i=1}^{s_c} \gamma_{l,i}x_i = X\gamma_l, \quad (16)$$

where  $\gamma_l = [\gamma_{l,1}, \dots, \gamma_{l,s_c}]^T \in R^{s_c}$  are the corresponding coefficient vector.

SRC has achieved remarkable results when there are sufficient training samples per subject. However, SRC relies on enough training samples of same category to achieve a good representation. Small training sample for this problem, a stable inverse projection-based PFSR [13] has been presented to effectively exploit complementary information between samples. In particular, useful information contained in the test sample set was excavated. And in the field of face recognition has achieved good results.

PFSR means that a training sample  $x_i$  from a category  $j$  is represented by its corresponding pseudo-full-space  $V_i = \{X, Y\} - \{x_i\}, i = 1, \dots, n$ .

$$x_i = \dots + \alpha_{j,i-1}x_{i-1} + \alpha_j x_{i+1} + \dots + \beta_{i,1}y_1 + \dots + \beta_{i,m}y_m = V_i z_i, \quad (17)$$

where  $\alpha_{i,j} \in R$  and  $\beta_{i,l} \in R$  are the corresponding coefficients before training samples and test samples respectively.  $z_i = [\alpha_{i,1}, \dots, \alpha_{i,n}, \beta_{i,1}, \dots, \beta_{i,m}]^T$  is the corresponding coefficient vector. The space  $V_i$  is the largest representation space of a sample  $x_i$ . Obviously,  $V_i$  provides richer information than the training sample space because of the addition of the test samples.

However, there is no obvious category-based complementary information in the gene expression profile data. Breast tumor gene recognition, the representation space

to add the training samples will produce interference information, the impact of the final classification. Therefore, we remove the training sample information in the PFSR representation space. A stable inverse projection represent has been presented to excavate the useful information contained in the test sample. Inverse projection represent is a special case of PFSR. Different application background, making the inverse projection representation and PFSR representation space is different. If the training sample space is null, pseudo-full-space is just the test sample space.

Inverse projection representation means that a training sample  $x_i$  is represented by its corresponding test sample space  $Y=[y_1, \dots, y_k]$ .

$$x_i = \alpha_{i,1}y_1 + \dots + \alpha_{i,l}y_l + \dots + \alpha_{i,k}y_k = \sum_{l=1}^k \alpha_{i,l}y_l = Y\alpha_i, \quad (18)$$

where  $\alpha_{i,l} \in R$  are representation coefficients. Let  $\alpha_i = [\alpha_{i,1}, \dots, \alpha_{i,l}, \dots, \alpha_{i,k}]^T$  represents coefficient vector.

Eq.(16), Eq.(17) and Eq.(18) are sparse representations, PFSR and inverse projection representation respectively. As can be seen from the representation, the representation space of the three representations is not the same.

### 2.3.2 IPSR model

Sparsity helps recognition the data class, in actual field there are obvious sparsity for breast tumor classification based on gene expression profile. The representation is obviously sparse, and the sparser the representation coefficient vector is, the easier it is to recognize the test samples category label. Therefore, we consider the sparsity constraints in inverse projection representation, called IPSR model. Let  $x \in X$  represents any training sample, IPSR codes  $x$  over a dictionary  $Y$  such that  $x = Y\alpha$  and  $\alpha$  is a sparse vector. The sparsity of  $\alpha$  can be measured by  $l_0$ -norm. Since the combinatorial  $l_0$ -minimization is NP-hard, the  $l_1$ -minimization, as the closest convex function to  $l_0$ -minimization, is widely employed in sparse coding:

$$\min_{\alpha} \|x - Y\alpha\|_2^2 + \lambda \|\alpha\|_1, \quad (19)$$

where  $\lambda$  is regularization parameter, and  $\alpha$  is the representation coefficient vector of  $x$ .

The model (19) is called IPSR model, IPSR can be more easily implemented than standard sparse representation. What we emphasize is that, the representation space may be enlarged with the help of test samples, especially there are a small number of training samples per category. Comparing Figs. 2 (a), (b) and (c), when we analyze test samples, it is easy to notice that the latter focuses on the column coefficients before test samples, rather than row coefficients of training samples for the former. The different projection way makes the inverse projection representation is less sensitive to the number of training samples than that of sparse representation. In the test sample with the help of mining hidden in the test sample helps to categorize information.

(a)

(b)

(c)

Fig.2 Comparison of different representation ways. (a) standard sparse representation, (b) PFSR, (c) IPSR.

### 2.3.3 Optimization IPSR model by GADMM

ADMM attracts a great deal of attention in biostatistics. It mainly deals with convex optimization problems with constraints. Algorithm termination criteria can be set based on the precision required, which is critical in large-scale data processing. Xiao et al. verified that the convergence error is less than classic ADMM and the convergence speed is faster than classic ADMM [41]. Therefore, this paper uses GADMM to optimize IPSR model, in order to obtain more accurate convergence solution.

Model (19) added constraints

$$\min_{\alpha} \|x - Y\alpha\|_2^2 + \lambda \|b\|_1 \quad s.t. \quad \alpha - b = 0. \quad (20)$$

For  $x \in R^{m \times 1}$ ,  $Y \in R^{m \times n}$ , the augmented Lagrangian function of problem (20) is defined as,

$$L_{\sigma}(\alpha, b; \eta) = \|x - Y\alpha\|_2^2 + \lambda \|b\|_1 + \langle \eta, \alpha - b \rangle + \frac{\sigma}{2} \|\alpha - b\|_2^2, \quad (21)$$

Let  $\sigma > 0$  be the penalty parameter,  $\eta \in R^{k \times 1}$  is the Lagrange multiplier,  $\langle \cdot, \cdot \rangle$  is the inner product.

The GADMM scheme takes the following form

$$\begin{cases} \alpha^k = \arg \min_{\alpha} L_{\sigma}(\alpha, \tilde{b}^k; \tilde{\eta}^k) + \frac{1}{2} \|\alpha - \tilde{\alpha}^k\|_K^2, & (a) \\ \eta^k = \tilde{\eta}^k + \sigma(\alpha^k - \tilde{b}^k), & (b) \\ b^k = \arg \min_b L_{\sigma}(\alpha^k, b; \eta^k) + \frac{1}{2} \|b - \tilde{b}^k\|_T^2, & (c) \\ \tilde{w}^{k+1} = \tilde{w}^k + \rho(w^k - \tilde{w}^k). & (d) \end{cases} \quad (22)$$

where  $w^k = (\alpha^k, b^k, \eta^k)$ ,  $\alpha^{-1} = \tilde{\alpha}^0$  and  $b^{-1} = \tilde{b}^0$ ,  $K : R^{k \times 1} \rightarrow R^{k \times 1}$  and

$T : R^{k \times 1} \rightarrow R^{k \times 1}$  are two semi-proximal matrix. The more natural choice for the

semi-proximal terms to be added will be  $\frac{1}{2} \|\alpha - \tilde{\alpha}^k\|_K$  and  $\frac{1}{2} \|b - \tilde{b}^k\|_T$  to the

sub-problems for computing  $\alpha^k$  and  $b^k$ . In [41], for the sake of generality and

numerical convenience, they consider the latter variant with only semi-proximal terms.

The most recent values of the variables are used in the proximal terms.

Sub-problem  $\alpha^k$  can be approximated by

$$\begin{aligned} \alpha^k &= \arg \min_{\alpha} \|x - Y\alpha\|_2^2 + \frac{\sigma}{2} \left\| \alpha - \tilde{b}^k + \frac{\tilde{\eta}^k}{\sigma} \right\|_2^2 + \frac{1}{2} \|\alpha - \tilde{\alpha}^k\|_K^2, \\ &= \arg \min_{\alpha} \left\langle Z^k, \alpha - \tilde{\alpha}^k \right\rangle + \frac{\theta_K}{2} \|\alpha - \tilde{\alpha}^k\|_2^2, \\ &= \arg \min_{\alpha} \frac{\theta_S}{2} \left\| \alpha - \tilde{\alpha}^k + \frac{Z^k}{\theta_K} \right\|_2^2. \end{aligned}$$

$$Z^k = Y^T x - Y^T Y \tilde{\alpha}^k - \sigma \tilde{b}^k + \sigma \tilde{\alpha}^k - \tilde{\eta}^k,$$

$$\alpha = \tilde{\alpha}^k - \frac{Y^T x - Y^T Y \tilde{\alpha}^k - \sigma \tilde{b}^k + \sigma \tilde{\alpha}^k - \tilde{\eta}^k}{\theta_K}. \quad (23)$$

where  $Y^T Y + \sigma I = K$ ,  $\theta_K > \|K\|^2$ .

Sub-problem  $b^k$  can be approximated by

$$\begin{aligned} b^k &= \arg \min_b \lambda \|b\|_1 + \langle \eta^k, \alpha^k - b \rangle + \frac{\sigma}{2} \|\alpha^k - b\|_2^2 + \frac{1}{2} \|b - \tilde{b}^k\|_T^2, \\ &= \arg \min_b \lambda \|b\|_1 + \frac{\sigma}{2} \left\| \alpha^k - b + \frac{\eta^k}{\sigma} \right\|_2^2 + \frac{1}{2} \|b - \tilde{b}^k\|_T^2, \end{aligned}$$

where  $T = 0$ , then

$$\begin{aligned} b^k &= \arg \min_b \lambda \|b\|_1 + \frac{\sigma}{2} \left\| \alpha^k - b + \frac{\eta^k}{\sigma} \right\|_2^2, \\ &= S_{\lambda/\sigma} \left( \alpha^k + \frac{\eta^k}{\sigma} \right). \end{aligned} \quad (24)$$

where  $S$  is a soft threshold function, similar to Ep.(9).

---

Algorithm: Optimization of IPSR based on GADMM

---

**Input:** Training samples matrix  $x \in [x_1, \dots, x_n]$ ,  $x \in \mathbb{R}^{m \times 1}$ , test samples matrix  $Y = [y_1, \dots, y_k]$ .

Set  $\rho \in (0, 2)$  and  $\sigma > 0$ .

**Initialize:** Initialize  $(\tilde{\alpha}^0, \tilde{b}^0, \tilde{\eta}^0) = (0, 0, 0)$ ,  $k = 0$ ,  $Y^T Y + \sigma I = K$ ,  $\theta_K > \|K\|^2$ .

**Iterate until convergence**

$$1) \quad \alpha^k = \tilde{\alpha}^k - \frac{Y^T x - Y^T Y \tilde{\alpha}^k - \sigma \tilde{b}^k + \sigma \tilde{\alpha}^k - \tilde{\eta}^k}{\theta_K},$$

$$2) \quad \eta^k = \tilde{\eta}^k + \sigma(\alpha^k - \tilde{b}^k),$$

$$3) \quad b^k = S_{\lambda/\sigma} \left( \alpha^k + \frac{\eta^k}{\sigma} \right),$$

$$\tilde{w}^{k+1} = \tilde{w}^k + \rho(w^k - \tilde{w}^k),$$

$$k = k + 1.$$

**End while**

**Output** An optimal solution.

---



### 2.3.4 Convergence analysis

In this section, the corresponding convergence analysis is achieved, which contains the convergence theorem and two lemmas. In order to prove the theorem, Karush-Kuhn-Tucker (KKT) for model (20) is given first.

Let  $f(\alpha) = \|x - Y\alpha\|_2^2$ ,  $g(b) = \lambda \|b\|_1$ , a vector  $(\tilde{\alpha}, \tilde{\eta}, \tilde{b})$  is said to be a saddle point to the Lagrangian function (21) if it is a solution to the following KKT system

$$\eta \in \partial f(\alpha), \quad -\eta \in \partial g(b), \quad \text{and} \quad \alpha - b = 0. \quad (25)$$

For the further discussions, we use the notations that  $\alpha_{<i} := (\alpha_1, \dots, \alpha_{i-1})$ ,  $\alpha_{>i} := (\alpha_{i+1}, \dots, \alpha_p)$  and similar notations for  $b$ . Let  $f(\alpha) = \sum_{j=1}^q f_j(\alpha_j)$ , recorded as  $\Sigma_f$ ,  $g(\alpha) = \sum_{j=1}^q g_j(b_j)$ ,  $1 \leq j \leq q$ , recorded as  $\Sigma_g$ . And conditional requirements [41]  $\Sigma_f + K > 0$  and  $\Sigma_g + T - I > 0$ .

For this purpose, we need the following two basic equalities:

$$2\langle u_1 - u_2, G(v_1 - v_2) \rangle = \|u_1 - v_2\|_G^2 - \|u_1 - v_1\|_G^2 + \|u_2 - v_1\|_G^2 - \|u_2 - v_2\|_G^2, \quad (26)$$

and

$$2\langle u_1 - Gu_2 \rangle = \|u_1\|_G^2 + \|u_2\|_G^2 - \|u_1 - u_2\|_G^2 = \|u_1 + u_2\|_G^2 - \|u_1\|_G^2 - \|u_2\|_G^2, \quad (27)$$

where  $u_1, u_2, v_1, v_2$  are vectors, and  $G$  is an arbitrary self-adjoint positive semi definite linear operator from that space to itself.

Next, let  $(\bar{\eta}, \bar{\alpha}, \bar{b})$  be an arbitrary solution to the KKT system (25). For any  $(\eta, \alpha, b)$  we denote  $\eta_e = \eta - \bar{\eta}$ ,  $\alpha_e = \alpha - \bar{\alpha}$  and  $b_e = b - \bar{b}$ . In order to give the convergence theorem of the GADMM optimization IPSR model, two lemmas are given first.

**Lemma 2.1** Let  $(\bar{\eta}, \bar{\alpha}, \bar{b})$  be a solution to the KKT system (25) and  $(\eta^k, \alpha^k, b^k)$  be the sequence generated by Eq. (22). For any  $k \geq 0$  it holds that

$$\langle \eta^{k+1} - \eta^k, \alpha^{k+1} - \alpha^k \rangle - \frac{\rho}{2} \|\alpha^{k+1} - \tilde{\alpha}^{k+1}\|_K^2 + \frac{\rho}{2} \|\alpha^k - \tilde{\alpha}^k\|_K^2 \geq \|\alpha^{k+1} - \alpha^k\|_{\Sigma_f}^2, \quad (28)$$

and

$$\begin{aligned} & \frac{\sigma\rho}{2} \|\alpha_e^{k+1} - b_e^k\|^2 + \langle \eta_e^{k+1} + \sigma(1-\rho)\alpha_e^{k+1}, \alpha_e^{k+1} - b_e^k \rangle \\ &= -\frac{1}{2\sigma\rho} \left[ \|\eta_e^{k+1} + \sigma(1-\rho)\alpha_e^{k+1}\|^2 - \|\eta_e^{k+1} + \sigma(1-\rho)\alpha_e^k\|^2 \right]. \end{aligned} \quad (29)$$

**Lemma 2.2** Suppose Eq. (22) holds. Let the sequence  $\{(\eta, \alpha, b)\}$  be generated by Eq. (22). Then for any  $k \geq 0$  it holds that

$$\begin{aligned} \phi_k - \phi_{k+1} &\geq 2\|\alpha_e^k\|_{\Sigma_f}^2 + 2\|b_e^k\|_{\Sigma_g}^2 + \sigma(2-\rho)\|\alpha_e^{k+1} - b_e^k\|^2 \\ &\quad + (2-\rho)\|\tilde{\alpha}^{k+1} - \alpha^{k+1}\|_K^2 + (2-\rho)\|\tilde{b}^k - b^k\|_T^2 \\ &\quad + 2(2-\rho)\rho^{-1}\|\alpha^{k+1} - \alpha^k\|_{\Sigma_f}^2 + \sigma\rho^{-1}(2-\rho)^2\|\alpha_e^k - \alpha_e^{k+1}\|^2. \end{aligned} \quad (30)$$

Now, we are ready to establish the global convergence of Eq. (22).

**Theorem 2.1** Suppose there exists a vector  $(\tilde{\alpha}, \tilde{\eta}, \tilde{b})$  satisfying the KKT system. Let  $\{(\eta^k, \alpha^k, b^k)\}$  be the sequence generated by Eq. (22). Then the whole sequence  $\{(\eta^k, \alpha^k, b^k)\}$  converges to a solution to the KKT system.

*Proof:* Note that  $\rho \in (0, 2)$ . We clearly see from (30) that  $\{\phi_k\}_k \geq 0$  is a nonnegative and monotonically non-increasing sequence. Hence,  $\{\phi_k\}$  is also bounded. As a result, the following sequences are bounded:

$$\left\{ \|\eta_e^k + \sigma(1-\rho)\alpha_e^k\| \right\}, \left\{ \|\tilde{\alpha}^{k+1}\|_K \right\}, \left\{ \|\tilde{b}^k\|_T \right\}, \left\{ \|\alpha^k - \tilde{\alpha}\|_K \right\}, \text{ and } \left\{ \|\alpha_e^k\| \right\}. \quad (31)$$

Moreover, from the inequality (31) we have as  $k \rightarrow \infty$ ,

$$\begin{aligned} & \|\alpha_e^{k+1}\|_{\Sigma_f} \rightarrow 0, \quad \|b_e^k\|_{\Sigma_g} \rightarrow 0, \quad \|\alpha_e^{k+1} - b_e^k\| \rightarrow 0, \quad \|\tilde{\alpha}^{k+1} - \alpha^{k+1}\|_K \rightarrow 0, \\ & \|\tilde{b}^k - b^k\|_T \rightarrow 0, \quad \|\alpha^{k+1} - \alpha^{k+1}\|_{\Sigma_f} \rightarrow 0 \text{ and } \|\alpha_e^k - \alpha_e^{k+1}\| \rightarrow 0. \end{aligned} \quad (32)$$

Thus, by the fact  $\|\alpha^k\|_K \leq \|\alpha^k - \tilde{\alpha}\|_K + \|\tilde{\alpha}\|_K$  we can see that  $\{\|\alpha^k\|_K\}$  is also bounded. Consequently, the sequence  $\{\|\alpha^k\|_{\Sigma_f+K}\}$  is bounded. Since  $\Sigma_f + K > 0$ , the

sequence  $\{\|\alpha^k\|\}$  is bounded. Similarly, the sequences  $\{\|b^k\|_T\}$  and  $\{\| -b^k\|\}$  are both bounded and so is the sequence  $\{\|b^k\|_{\Sigma_g+T-I}\}$ . It implies that the sequence  $\{\|b^k\|\}$  is bounded from  $\Sigma_g+T-I>0$ . The boundedness of  $\{\|\eta_e^k + \sigma(1-\rho)\alpha_e^k\|\}$  and  $\{\|\alpha^k\|\}$  further indicate that the sequence  $\{\|\eta^k\|\}$  is bounded. The above arguments have shown that  $\{(\eta^k, \alpha^k, b^k)\}$  is a bounded sequence.

Consequently, the sequence  $\{(\eta^k, \alpha^k, b^k)\}$  admits at least one convergent subsequence. Suppose that  $\{(\eta^{k_i}, \alpha^{k_i}, b^{k_i})\}$  is a subsequence of  $\{(\eta^k, \alpha^k, b^k)\}$  converging to  $\{(\eta^\infty, \alpha^\infty, b^\infty)\}$ . It follows from (22b) that

$$\eta^k - K(\alpha^k - \tilde{\alpha}^k) \in \partial f(\alpha^k), \text{ and } \eta^{k+1} - K(\alpha^{k+1} - \tilde{\alpha}^{k+1}) \in \partial f(\alpha^{k+1}), \quad (33)$$

And we get from (22c)

$$-\eta^{k+1} + (-\eta^k + \eta^{k+1}) + \sigma(\alpha^k - b^k) - T(b^k - \tilde{b}^k) \in \partial g(b^k), \quad (34)$$

It follows from (33) and (34) that

$$\begin{cases} \eta^{k_i} - K(\alpha^{k_i} - \tilde{\alpha}^{k_i}) \in \partial f(\alpha^{k_i}), \\ -\eta^{k_i} + \sigma(\alpha^{k_i} - b^{k_i}) - T(b^{k_i} - \tilde{b}^{k_i}) \in \partial g(b^{k_i}). \end{cases} \quad (35)$$

We also have from (32) that  $\lim_{k \rightarrow \infty} (\alpha^k - b^k) = 0$ . Taking limits in (32) and using (35), one obtains

$$\eta^\infty \in \partial f(\alpha^\infty), \quad -\eta^\infty \in \partial g(b^\infty) \text{ and } \alpha^\infty - b^\infty = 0,$$

which indicates that  $(\eta^\infty, \alpha^\infty, b^\infty)$  is a solution to the KKT system (25).

Next we need to show that  $(\eta^\infty, \alpha^\infty, b^\infty)$  is the unique limit point of the sequence  $\{(\eta^k, \alpha^k, b^k)\}$ . Without loss of generality we can let  $(\bar{\eta}, \bar{\alpha}, \bar{b}) = (\eta^\infty, \alpha^\infty, b^\infty)$ . Consequently, the sequence  $\{\phi_k\}$  itself converging to zero. By the definition of  $\phi_k$  we have  $\lim_{k \rightarrow \infty} \eta^k = \bar{\eta}$ . Moreover, from  $\|\tilde{\alpha}^{k+1} - \alpha^{k+1}\|_K \rightarrow 0$  in (32), it is easy to show that  $\|\alpha_e^k\|_K \rightarrow 0$  as  $k \rightarrow \infty$ . Noting that  $\|\alpha_e^k\|_K \rightarrow 0$  in (31) and  $\|\alpha_e^k\|_{\Sigma_f} \rightarrow 0$  in (32),

we have  $\left\{\|\alpha_e^k\|_{\Sigma_f} + \|\alpha_e^k\|_K + \|\alpha_e^k\|\right\} \rightarrow 0$  as  $k \rightarrow \infty$ . Hence, we have  $\lim_{k \rightarrow \infty} \alpha^k = \bar{\alpha}$  since  $\Sigma_f + K > 0$ . Finally, from the fact  $\|\alpha_e^{k+1}\| \rightarrow 0$ ,  $\|\alpha_e^{k+1} - b_e^k\| \rightarrow 0$  in (32), and

$$\| -b_e^k \| \leq \| \alpha_e^{k+1} - b_e^k \| + \| \alpha_e^{k+1} \|.$$

We get  $\| -b_e^k \| \rightarrow 0$ . Since  $\|b_e^k\|_T \rightarrow 0$  and  $\|b_e^k\|_{\Sigma_g} \rightarrow 0$  by (32), we have  $\left\{\|b_e^k\|_{\Sigma_g} + \|b_e^k\|_T + \| -b_e^k \|\right\} \rightarrow 0$  as  $k \rightarrow \infty$ . Therefore, from the fact  $\Sigma_g + T - I > 0$  we know that  $\lim_{k \rightarrow \infty} b^k = \bar{b}$ . This completes the proof.

Theorem 2.1 of the proof process, refer to the GADMM [41] convergence analysis. The theorem shows that if the solution of the model exists, the iterative solution satisfies the constraint condition. Furthermore, if the solution is unique, the iterative solution of each single variable converges to the real solution. In section 3.4, the experimental part gives the iterative error curve of LPML-SNMF model.

### 2.3.5 Classification

Similar to [13], because of the inapplicability and instability of reconstruction errors, the coefficient matrix obtained for the IPSRC model use the category contribution rate (CCR) as the classification criteria. For a test sample  $y_r$ , the contribution rate  $C_{j,r}$  of  $y_r$  for the  $j$ -th category can be calculated by

$$C_{j,r} = \frac{1}{s_j} \sum_i \left( \frac{\delta_j(\{\alpha_{i,r}\})}{\sum_i \{\alpha_{i,r}\}} \right), i = 1, \dots, s_1, \dots, s_c, \quad (36)$$

where  $\delta_j: R^n \rightarrow R^n$  is a characteristic function that selects coefficients associated with the  $j$ -th category. For  $x \in R^n$ ,  $\delta_j(\hat{\alpha})$  is a new vector whose only nonzero entries in  $\alpha$  that are associated with category  $j$ , where categories  $j = 1, \dots, c$ ,  $r = 1, \dots, k$ ,  $s_j$  denotes the number of  $j$ -th category training samples.

Through the CCR, we can compare correlations between each test sample and every category. The larger the CCR is, the higher the correlation is. A test sample  $y_r$

is classified into the category with the maximal CCR  $\{C_{j,r}, j = 1, \dots, c\}$

$$m_r = \arg \max_{j \in \{1, \dots, c\}} (C_{j,r}). \quad (37)$$

And categories of all test samples are obtained simultaneously and classification can be completed.

#### 2.4 Breast tumor classification

A breast tumor classification algorithm is introduced based on The DIF gene selection described above, LPML-SNMF feature selection and IPSRC. Fig. 3 shows the framework of the breast tumor classification, as can be seen from Fig. 3, the breast tumor classification is divided into three stages.

The first stage is DIF-based gene selection. Without loss of generality, we first make a primary selection of breast tumor data based on the accepted gene selection method BW. Second, the main information genes selection stage based on DIF. By this way, information genes for breast tumor classification can be obtained.

The second stage is LPML-SNMF-based feature selection. In order to dig more effectively breast tumor data in favor of classification information, relevant features selected for breast tumor classification. The decision information genes obtained by DIF are feature selected by LPML-SNMF.

The third stage is IPSRC-based classification. The features obtained by LPML-SNMF are based on the classification of breast tumor by IPSRC. The final features  $H_2$  of LPML-SNMF are divided into training set  $H_2^{training}$  and test set  $H_2^{test}$ ,  $H_2^{test}$  as the dictionary of IPSR represent  $H_2^{training}$ .

$$\min_{\alpha} \left\| (h_2)_i^{training} - H_2^{test} \alpha \right\|_2^2 + \lambda \|\alpha\|_1, \quad (38)$$

where  $H_2^{training} = [(h_2)_1^{training}, \dots, (h_2)_i^{training}, \dots, (h_2)_{s_c}^{training}]$ ,  $i = 1, \dots, s_c$ . The coefficient matrix is obtained through the optimization process in section 2.3.3  $A = [\alpha_1, \dots, \alpha_{s_c}]$ .

By Eq. (36), the CCR matrix is got, a test sample is classified into the category with the maximal CCR.

Combined the selected information gene with LPML-SNMF gene feature selection

and IPSRC, the basic process of our breast tumor classification algorithm is as follows.

---

Algorithm: Breast tumor classification algorithm

---

Input: Training sample set  $X = [x_1, \dots, x_n]$ , training label set  $L = [l_1, l_2, \dots, l_n]$  and test sample set  $Y = [y_1, y_2, \dots, y_k]$ .

Gene feature selection based on LPML-SNMF and classification based on IPSRC:

Step1. By Eq. (10) (11) (12), the first layer of LPML-SNMF gene feature selection is realized.

Step2. By Eq. (13) (14) (15), the second layer of LPML-SNMF gene feature selection learning is realized.

Step3. By Eq. (38), the inverse projection representation is realized, and where  $X = H_2^{train}$ ,

$$H_2^{train} = [(h_2^{train})_1, \dots, (h_2^{train})_n]. \quad Y = H_2^{test}, \quad H_2^{test} = [(h_2^{test})_1, \dots, (h_2^{test})_k].$$

Step4. By section 2.3.3 of the optimization process, the projection coefficient matrix is got.

Step5. By Eq. (36), the CCR matrix is got, and by normalizing the CCR matrix, relevancies between each test sample and all categories are obtained.

Output: By Eq. (37), each test sample can be classified into the category with the maximal CCR.

---

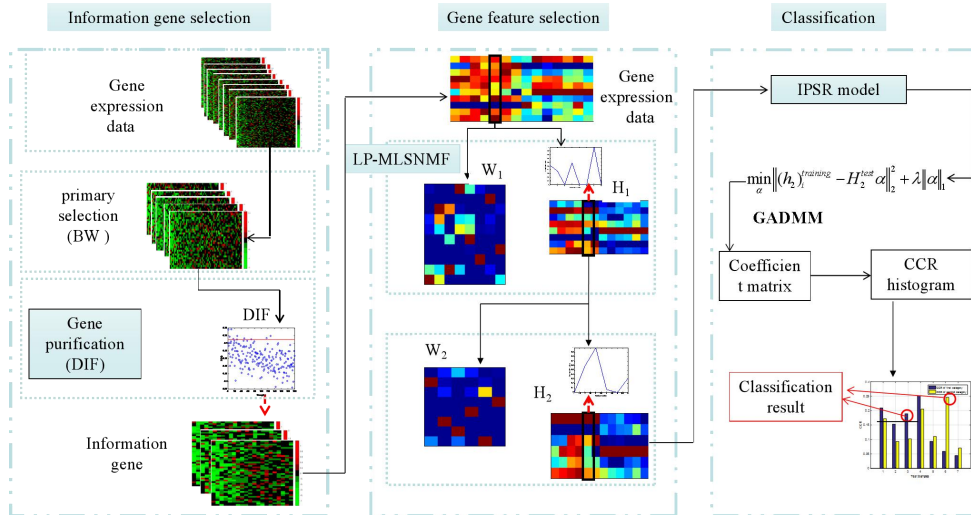


Fig.3 The framework of the breast tumor classification

### 3. Experiments and discussions

In this subsection, efficacy of the proposed method is demonstrated by extensive experiments on three breast tumor gene expression datasets. Seven sets of experiments are performed: feasibility analysis for DIF, classification performance analysis of information genes, performance of LPML-SNMF, convergence analysis of IPSRC, parameter analysis, breast tumor classification performance analysis and comparison, information genes biology analysis. For the Gene selection section, we compare it with the accepted BW [50], SNR [51], but also compared with the latest ROC [39] gene selection method proposed in 2017. Since LPML-SNMF is an improvement of SNMF [27] and ML-NMF [43], the gene signature section is compared with these two methods. Classification is not only compared with the traditional classification methods NN [52], SVM [28], CRC [31] and SRC [29]. The performance of IPSRC is also compared with the latest method based sparse representation. The compared methods are PFSRC [13], RRC\_L1 [32] and RRC\_L2 [32]. Fifteen kinds of measures are used to measure the performance of these methods. Classification of the angle of measurement tools are: Accuracy, sensitivity, specificity, positive predictive value and negative predictive value, Error reduction rate (ERR) [35]. The measurement tools used in clinical medicine: Receiver operating characteristic curve (ROC) [46], DCA [45]. Statistical tools for measuring the angle are: Heatmap, sparseness, correlation coefficient, box plots, equal value and direction difference, mutual information (MI), entropy etc. Without loss of generality, 10-fold cross-validation is used to test the performance of the algorithms. According to experience to obtain  $r_1 = 8, r_2 = 6$ .

All experiments are carried out using MATLAB R2016a on a 3.30GHz machine with 4.00GB RAM and R-3.4.1.

### 3.1 Breast tumor data sets

**Breast-2 [56]:** This breast tumor study was first reported in [56]. This DNA microarray analysis on primary breast tumors of 25,000 gene expression measurements of 117 young patients. We selected 79 primary breast tumor:34 from patients who developed distant metastases within 5 years,45 from patients who

continued to be disease-free after a period of at least 5 years. All 79 patients were lymph node-negative, and 55 years old or younger. From each patient, tumor size under 5cm. The patients who developed distant metastases within 5 years were recorded as tumor samples without any confusion, the patients who continued to be disease-free after a period of at least 5 years are called a normal sample.

**Breast-2(97) [25]:** For the samples of 117 databases Van't Veer et al[56], about 25,000 genes. Many articles select samples for further analysis and classification based on different indicators. Jiang et al. [25] Where 97 lymph node-negative breast tumor patients, 55 years old or younger, participated in this study. Among them, 46 developed distant metastases within 5 years and 51 remained metastases free for at least 5 years, which is reported as(Breast2(97)).

**Breast-2(77) [4]:** Fan et al.[4] chose 77 samples on the basis of Van't Veer et al [56] .There were 44 developed distant metastases within 5 years and 33 remained metastases free for at least 5 years, which is reported as (Breast 2 (77)).

### 3.2 Performance of gene selection based on DIF

In this subsection, the effectiveness and efficiency of the proposed information gene selection based on DIF method are demonstrated. The reasons for the primary selection of BW genes are as follows. The purification gene of breast tumor data analysis of decision curve. Then use the DIF of genes to sort and select the decision genes. The decision curve is an experiment conducted on the R software. Gene expression data is large, experimental workload, time-consuming. In order to reduce the computational complexity, we conduct primaries based on accepted gene selection method. We analyzed the feasibility of our gene selection method through interval distribution, sample visualization, ROC and DCA.

#### 3.2.1 Gene selection based on DIF

Information genes selection based on DIF, the larger a gene DIF, the more decision information is represented. Selection the top-ranked genes for gene feature selection and classification. The blue circles in Fig.4 indicate the DIF for each gene. Fig.4 shows that, most of the genes DIF are concentrated in the 0.11-0.2 interval. Information genes that affect breast tumor classification are relatively rare. In this



paper, we select 10 genes for further gene feature selection and classification. Then the information genes contains the genes (10 genes), which occur more than a threshold value.

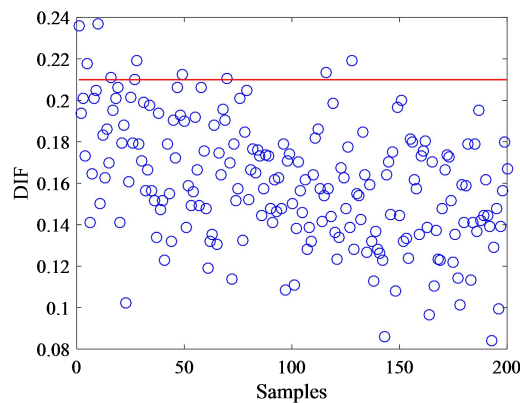


Fig.4 DIF value on Breast-2 dataset. In general, the more DIF value, the more important the gene is. The red line expresses the threshold of gene selection.

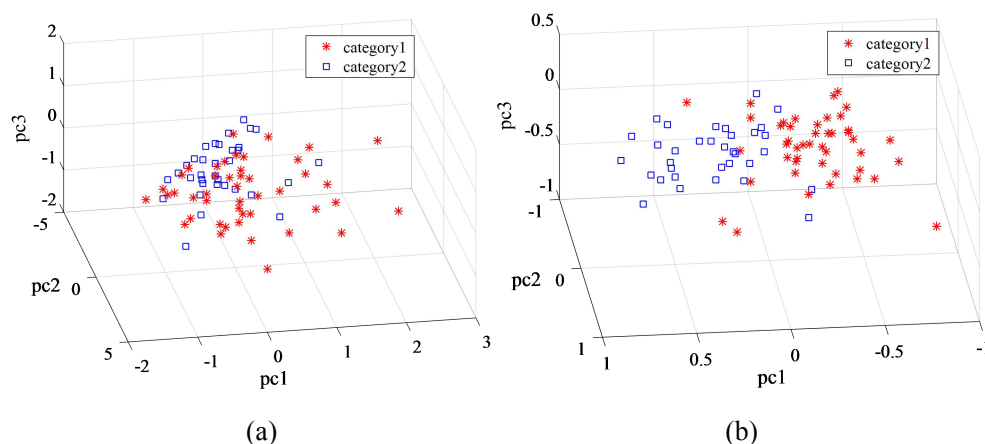


Fig.5 Representation of all samples consisting of 45 normal (red stars) and 34 tumor (blue squares) on Breast-2 datasets. (a) the top three components of BW gene primary selection 200 genes; (b) the top three components of 10 information genes

The performance of gene selection is visualized using principal component analysis. Fig.5 represents 79 samples consisting of 34 tumor (red stars) and 45 normal (blue squares) using the top three principal components of 200 genes based on BW gene primary selection and 10 information genes based on DIF respectively. Fig.5 (a) shows that a few of the 200 genes provide classification information and the distribution just looks uniform in each direction. Fig.5 (b) shows that the 10 information genes can mostly separate different tumors has the best separation performance than that of Fig.5(a). All this suggests that the information genes contain the main classification discriminant information.

Next, verify that the classification performance of the 10 information genes our method selected is actually better than the genes classification performance of BW, which is the accepted gene selection method. We use the DCA to measure the classification performance. Fig.6 shows that the DCA curve of BW selection 10 genes (blue representation) and our method DIF selection the 10 information genes (red representation). DCA represent the intersection threshold interval in the two extreme cases (gray). The higher the decision curve, the greater the net benefit and the higher the overall accuracy of the classification. Fig.6 show that red curves are higher than the blue curve in the threshold interval. Conclusions DCA can clearly see that the 10 information genes for our method selection are better than the 10 genes for BW selection.

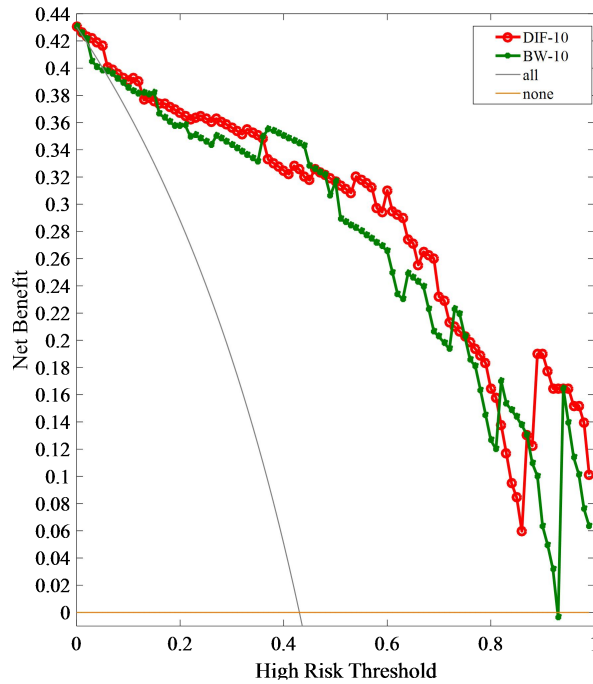


Fig.6 10 genes selected based DIF and 10 genes selected based BW on Breast-2 datasets

### 3.2.2 Breast tumor classification based on different gene selection methods

In addition to verifying the feasibility of DIF from the selected informational genes themselves, we also compare our method with some other accepted gene selection methods, including BW [50], SNR [51], which are also performed on Breast-2 databases. Table 1 proves that our algorithm is still competitive with higher accuracies than these methods. The same feature selection methods of genes for different methods of choice, and finally breast cancer classification based on

IPSRC. It can be seen from Table 1 that the classification performance of DIF is higher than the classification performance of SNR and BW under all feature selection cases. Especially, classification effect of LPML-SNMF feature selection,  $DIF(96.03\%) > ROC(88.59\%) > SNR(86.51\%) > BW(86.05\%)$ . Conclusion, the information genes based on DIF selection have greatly improved the classification performance.

Table.1 The accuracies based on IPSRC based on different gene selection methods

Gene selection methods	Accuracy(%)				
	None feature selection	SNMF[27]	ML-NMF[43]	ML-SNMF	LPML-SNMF
SNR[51]	62.76	65.12	76.89	78.611	86.51
BW[50]	61.15	67.70	79.72	81.15	86.05
ROC [39]	59.88	69.86	80.34	81.31	88.59
<b>DIF</b>	<b>70.97</b>	<b>77.14</b>	<b>84.94</b>	<b>87.94</b>	<b>96.03</b>

### 3.3 Performance of feature selection based on LPML-SNMF

In this subsection, the effectiveness and efficiency of the proposed gene feature selection method are demonstrated. We analyze the performance of LPML-SNMF by Heatmap, sparseness, convergence analysis, correlation, box plots, equal value and direction difference, k-means, MI, entropy etc. method. In an ambiguous situation,  $V$  represent matrix of all information genes,  $H_1$  represent the first layer hidden components matrix of LPML-SNMF,  $H_2$  represent the second hidden components matrix of LPML-SNMF

#### 3.3.1 Heatmap analysis

Heat map is an intuitive visualization method for analyzing the distribution of experimental data. It can be used for quality control of experimental data and visualization of differential data, and observation of sample quality. This section validates the feasibility of LPML-SNMF through heat map analysis. This section selection six tumor samples, six normal samples, and the first six samples are one

category and the last six samples are one category.

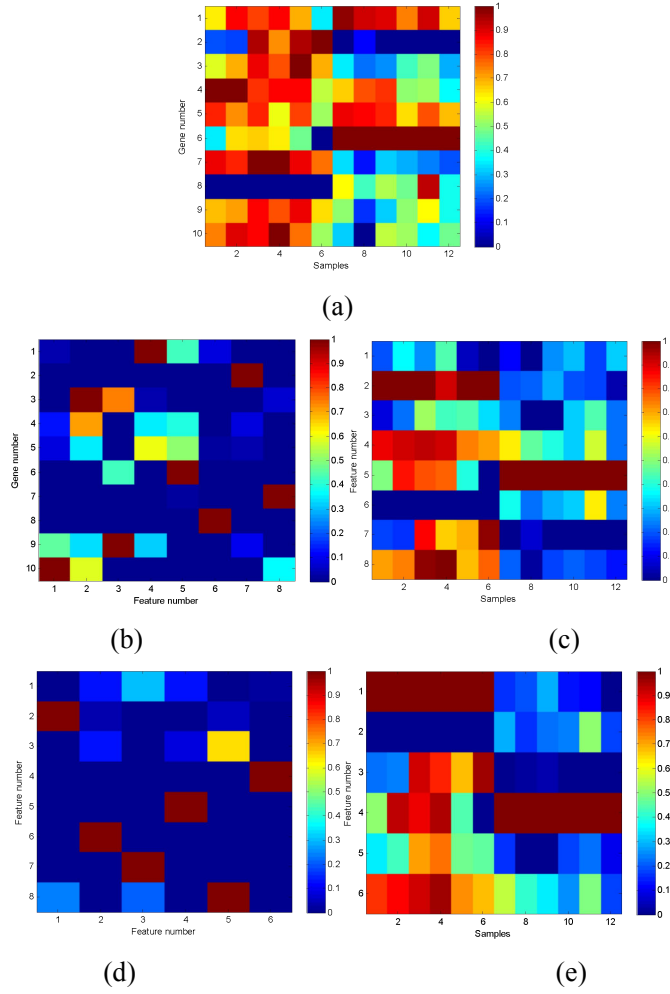


Fig.7. LPML-SNMF gene feature selection of the basis matrix, and the hidden components matrix. (a) The matrix of all information genes  $V$ , (b) The first layer basis matrix  $W_1$  of LPML-SNMF, (c) The first layer hidden components matrix  $H_1$  of LPML-SNMF, (d) The second layer basis matrix  $W_2$  of LPML-SNMF, (e) The second layer hidden components matrix  $H_2$  of LPML-SNMF.

Blue to red colors represents low to high expression levels of samples. Fig.7 shows the Heatmap for LPML-SNMF gene feature selection of the basis matrix and the hidden components matrix, where transition from blue to red colors corresponds to a shift from low to high expression values of the genes or features. Fig.7. (a) represent the matrix of all information genes  $V$ , Fig.7 (c) represent the first layer hidden components matrix  $H_1$  of LPML-SNMF, Fig.7(e) represent the second layer hidden components matrix  $H_2$  of LPML-SNMF. Fig.7 (a) (c) (e) can see that the layer of LPML-SNMF increased significantly in tumor and normal. The same category samples of the expression levels is getting closer and closer, and the difference

categories samples of expression levels is getting bigger and bigger.

### 3.3.2 Correlation analysis

Correlation analysis is a method of analyzing the correlation between variables. This section analyzes the Correlation of the LPML-SNMF features obtained for each layer. Suppose  $X=[x_1, \dots, x_m]$  and  $Y=[y_1, \dots, y_m]$ , correlation coefficient(CC) calculated as follows:

$$R = \frac{\sum_{i=1}^m (x_i - \bar{x})(y_i - \bar{y})}{\sqrt{\sum_{i=1}^m (x_i - \bar{x})^2 \cdot \sum_{i=1}^m (y_i - \bar{y})^2}}.$$

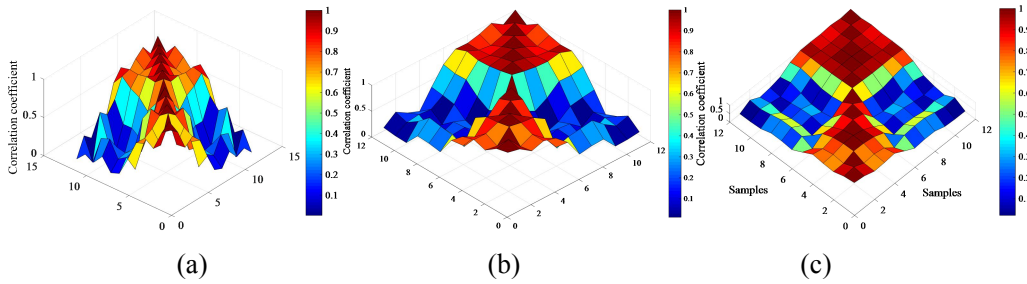


Fig.8 The CC between samples as a three-dimensional Heatmap. (a)the matrix of all information genes  $V$ , (b) the first layer hidden components matrix  $H_1$  of LPML-SNMF, (c) the second layer hidden components matrix  $H_2$  of LPML-SNMF.

Similar to section 3.3.1 selection six tumor samples, six normal samples, and the first six samples are one category and the last six samples are one category. Fig.9 shows that the CC between samples as a three-dimensional Heatmap. Blue to red colors represents low to high expression levels of samples CC. Fig.8 (a) represent the matrix of all information genes  $V$ , Fig.8 (b) represent the first layer hidden components matrix  $H_1$  of LPML-SNMF, Fig.8 (c) represent the second layer hidden components matrix  $H_2$  of LPML-SNMF. Fig.6 can be seen that the LPML-SNMF number of layers increases. Correlation of same category samples surface color gradually becomes dark red and the surface is more and more smooth, the correlation is getting higher and higher. Similar to correlation of different category samples surface color gradually becomes blue and the surface is more and more smooth, the correlation is getting lower and lower. Conclusion, the correlation between the samples of the same category is large, and between the samples of different category

is small.

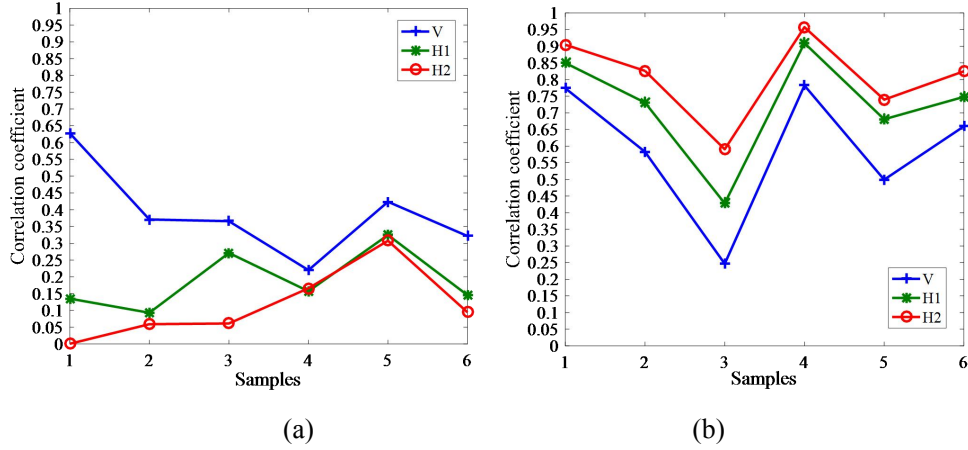


Fig.9 Features Correlation Coefficients of LPML-SNMF each layerline chart.12 samples (6 tumor samples and 6 normal samples) and 45 normal samples of the mean sample correlation analysis, analysis of their relevance.(a) The Correlation Coefficients of 6 tumor samples and the mean sample, (b) The Correlation Coefficients of 6 normal samples and the mean sample

In order to further verify that LPML-SNMF can improve classification performance. All samples (79) and 45 normal samples of the mean sample correlation analysis, analysis of their relevance. In order to clearly show the results, selection the same sample as section 3.3.1. Fig.10 represent the correlation of each layer feature obtained from LPML-SNMF of 12 samples and the mean sample, and the original data  $V$  (blue line), first layer feature  $H_1$  (green line), second layer feature  $H_2$  (red line). Where the first six are tumor samples and the last six are normal samples. Fig.9 represents that the correlations of the features of the each layer in the first six tumor samples are lower than those of the last six normal samples. Further verify the correlation between the same categories, small correlation between different categories. The first six samples LPML-SNMF feature correlation decreases with the number of layers increases, and  $H_2$  (red line) has the lowest correlation. The last six samples LPML-SNMF feature correlation increases with the number of layers increases, and  $H_2$  (red line) has the largest correlation. It verify that LPML-SNMF cause the correlation between the same category gradually increased, the correlation between different categories gradually reduced. Conclusion, the samples correlation of LPML-SNMF gets more and more significant as the number of layers increases. And the greater the correlation between same category, the smaller the correlation

between different category, the resulting classification performance will get better and better.

### 3.3.3 Box plots analysis

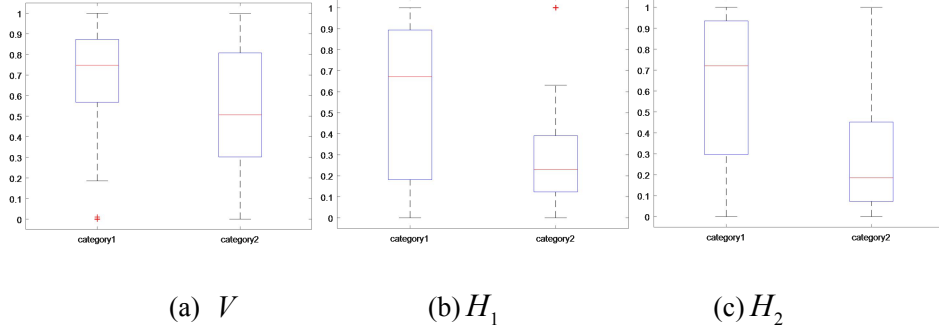


Fig.10 LPML-SNMF features of each layer box plots

Fig.10 represents the corresponding box plots to verify the feasibility of LPML-SNMF features for both normal and tumor breast tumor classification problems. Selection the same sample as section 3.3.1. Fig.10 represents box plots of the original data  $V$  (a), first layer feature  $H_1$  (b), second layer feature  $H_2$  (c). Namely, box's location and scale indicate the median (red lines) and interquartile range (blue box), respectively, and the bias of the distribution is mainly from the median. Fig.10 represents the LPML-SNMF features obtained as the number of layers increases, the median of the two categories of samples is farther and farther apart. And the expression level of tumor samples is getting lower and lower. Conclusion, the features obtained by LPML-SNMF contribute to the improvement of classification performance.

### 3.3.4 Performance analysis of LPML-SNMF

This section verifies the classification performance of LPML-SNMF in five different methods. (i) Variance: According to the training sample data, the mean and variance of each category of samples are calculated. Each test sample is added to two categories of training sample data, the test sample is divided into small changes in the category of variance. (ii) K-means clustering directly clustering  $V$ ,  $H_1$ ,  $H_2$  to compare the clustering accuracy. (iii) MI (Mutual Information) do classification, MI describes the correlation between the two variables, or the amount of information that

each contains. The larger the MI, the larger the correlation between the two variables. Based on the training samples, the mean samples of each category of samples is calculated. Then, calculation the MI for each test sample and each mean sample, and divide the test sample into the category with the larger MI. (iv) Entropy is a measure of system uncertainty that reflects the total amount of information a system can provide. The greater the entropy, the greater the degree of confusion and the greater the uncertainty.

Table 2 and Fig.11 represent the results of the above five methods, LPML-SNMF feature classification performance getting better and better. For example k-means,  $V$  clustering accuracy 58.43%,  $H_1$  clustering accuracy 84.81%,  $H_2$  clustering accuracy 86.58%.LPML-SNMF ultimate feature  $H_2$  highest accuracy. Conclusion, the feature classification obtain by LPML-SNMF is the best.

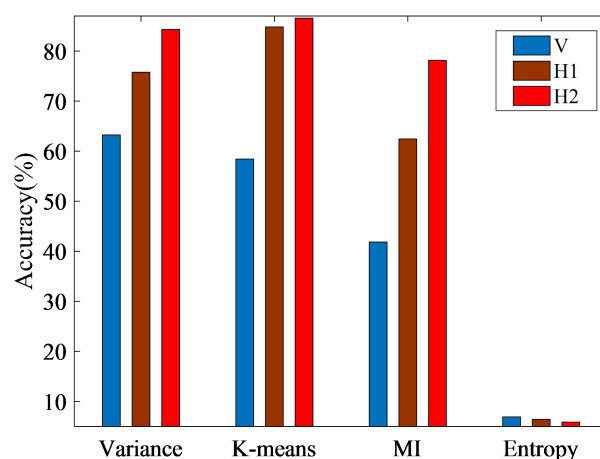


Fig.11 Histogram of five methods to measure the LPML-SNMF obtained the features of each layer

Table.2 Five methods to measure the LPML-SNMF obtained the features of each layer



Database	Methods	Variance	k-means	MI	Entropy
Accuracy(%)					
Breast-2	$V$	63.24	58.43	41.85	6.9028
	$H_1$	75.76	84.81	62.44	6.4218
	$H_2$	<b><u>84.31</u></b>	<b><u>86.58</u></b>	<b><u>78.14</u></b>	<b><u>5.8691</u></b>

### 3.3.5 Regularization parameters analysis

As shown in Subsection 2.2.2, in LPML-SNMF model (8) and (9), where  $\lambda_1$  and  $\lambda_2$  are  $l_1$ -norm regularization parameters and control the sparsity of matrix  $H_1$  and  $H_2$ , respectively. And satisfies  $1 > \lambda_1, \lambda_2 > 0$ , since the sparsity of the matrices obtained by LPML-SNMF decomposition has a very important role in classifying learning, the value of  $\lambda_1, \lambda_2$  has a great effect on the result. Therefore, the setting of this set of parameters is tested, and the appropriate  $\lambda_1, \lambda_2$  is selected through the experimental results.

The features obtained for LPML-SNMF are based on the IPSRC breast tumor classification. Selection  $\lambda_1=0.0, 0.2, 0.5, 0.7, 0.9$ ,  $\lambda_2=0.0, 0.2, 0.5, 0.7, 0.9$  in the case of the same initial value  $W_1^0, W_2^0, H_1^0, H_2^0$ . Testing the effects of the change of sparse constraint parameters on the classification results, and test each group of data. For the comparability of experimental results, all experiments in the same set of data are carried out under the same condition.

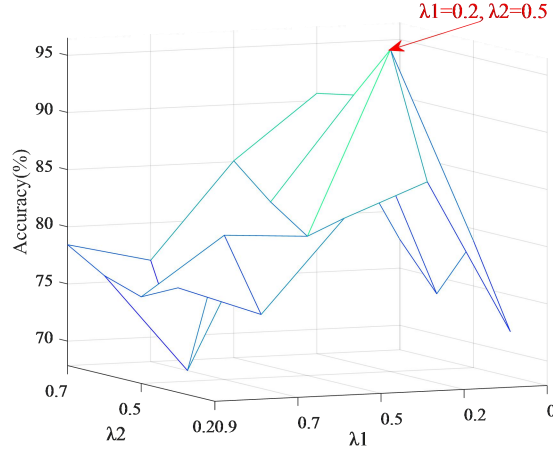


Fig.12 Accuracies based on IPSRC with different  $\lambda_1, \lambda_2$  three-dimensional surface on Breast-2 dataset.

Fig.12 represent the accuracy results of different regularization parameters  $\lambda_1$  and  $\lambda_2$ . The experimental results show that the values of regularization parameters  $\lambda_1$  and  $\lambda_2$  have a great influence on the classification results. The feature obtained by LPML-SNMF are not as sparse as possible, its sparse degree of serious impact on the final classification results. Therefore selection the best value of  $\lambda_1$ ,  $\lambda_2$  is very important. Fig.12 represent when  $\lambda_1=0.2$ ,  $\lambda_2=0.5$ , the classification result is the best. Therefore, selection the regularization parameter  $\lambda_1=0.2$ ,  $\lambda_2=0.5$  uniformly in our experiment.

### 3.4 Breast tumor classification based IPSRC

In this section, we verify IPSRC-based breast tumor classification performance. First, the convergence of IPSR optimization by GADMM solution is verified. Secondly, by comparing the classical classification methods NN [52], SVM [28], CRC [31] and SRC [29] and the new SRC improvement methods PFSRC [13], RRC\_L1 [32] and RRC\_L2 [32]. Validating the validity of IPSRC for breast tumor classification. Without loss of generality, on the basis of the experiments in sections 3.2 and 3.3, information gene selection based DIF, and feature selection based LPML-SNMF. The resulting features were imported into different classifiers for breast tumor classification.

### 3.4.1 Convergence analysis of IPSRC optimization by GADMM

In Section 2.3.2, we adoption GADMM to solve the IPSRC model. Xiao et al in [41] article has proved that GADMM is convergent. In this section, validation in solving the IPSRC model, GADMM is superior to classic ADMM in terms of convergence rate and error.

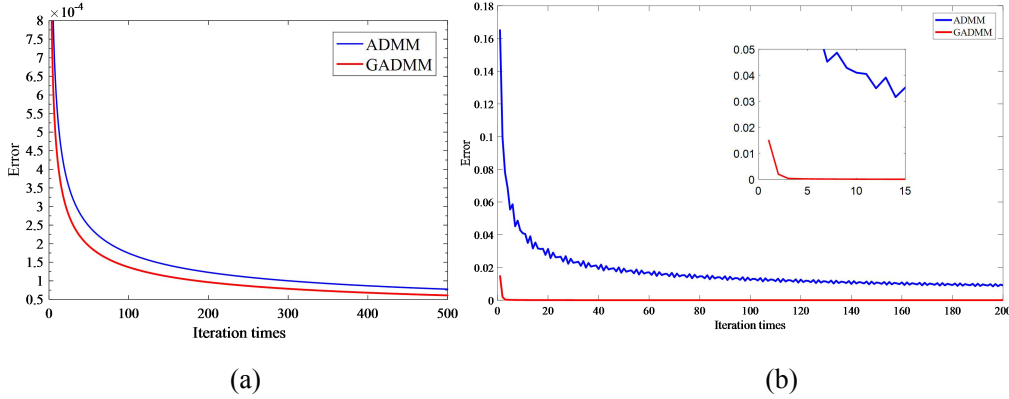


Fig.13 Convergence analysis between ADMM algorithm and GADMM algorithm.(a) The iteration error chart between exact solution and iterative solution; (b) The iteration error chart between adjacent iterations.

Fig.13 represent two algorithms ADMM and GADMM iterative error chart for solving IPSRC model. Where Fig.13 (a) the iteration error chart between exact solution and iterative solution, Fig.13 (b) The iteration error chart between adjacent iterations. We can be seen from Fig.13 the iterative rate shows that GADMM (red line) is faster than ADMM (blue line). And the convergence error of the GADMM is less than the convergence error of the ADMM. Fig.14 (a) represent the convergence error of ADMM is about  $10e-5$ , and iteration convergence times is about 150. The convergence error of GADMM is about  $1e-5$ , and iteration convergence times is about 100. Fig.13 (b) represent the convergence error of ADMM is about 0.02, and iteration convergence times is about 100. The convergence error of GADMM is about 0, and iteration convergence times is about 3. Conclusion, in solving the IPSRC model, GADMM is superior to classic ADMM in terms of convergence. Therefore, breast tumor classification, we use GADMM to solve the IPSRC model.

### 3.4.2 Performance of IPSRC based breast tumor classification

In this subsection, the effectiveness and efficiency of the proposed IPSRC methods are demonstrated. Based on previous gene selection and feature extraction, testing

IPSRC-based breast classification results. Since IPSRC is essentially an improvement of SRC, in this section, we compare the effectiveness of IPSRC with various SRC. And verify IPSRC based on different method characteristics due to SRC.

The classification results, accuracy, sensitivity, specificity, positive predictive value and negative predictive value are listed in Table 3, 4, 5. First, table 3, 4, 5 show that IPSRC achieves competitive results with highest accuracy, sensitivity, specificity, positive predictive value and negative predictive value based on different feature selection, which show IPSRC has the best prediction ability among the two classifiers. And IPSRC accuracy reaches up to 96.03% under LPML-SNMF feature selection. In conclusion, the classification result of IPSRC is higher than that of SRC, and it is indirectly verified that the classification effect of LPML-SNMF is best in these feature selection methods.

Breast tumor is the most common malignant tumor in women and is the second factor in female mortality. Early in the clinic a clear diagnosis of the latter part of the treatment and prognosis is crucial, so the lower the rate of missed diagnosis, the better. Missed diagnosed is greatly reduced, providing a more powerful diagnostic technique for the early detection of breast tumor, early diagnosis and early treatment. For the Breast-2 data, our method missed diagnosed of 2.5%. The problem with the clinical diagnosis of Breast tumor is the lack of specificity. Our method specificity of 94.17%, misdiagnosis 5.83%. Our method have achieved the better results in terms of sensitivity and specificity. As for the acceptable level of accuracy, sensitivity and specificity for a given disease depend on clinical context. Generally speaking, the stronger they are, the bigger the clinical significance is. Consequently we can draw the conclusion that the results of IPSRC are in the acceptable range.

For the feature selection LPML-SNMF, measuring classification performance of IPSRC and SRC models by drawing ROC and DCA. The area under the ROC curve is AUC, the larger the AUC value, and the closer the curve is to the upper left corner, the better the classification effect of the representative model. Between the model's DCA curve and the intersection of the all and none lines, the higher the model curve represents the better the classification. As can be seen from Fig.14, the red (IPSRC)

line is better than the blue (SRC) line classification. And  $AUC_{SRC} = 0.9059 < AUC_{IPRC} = 0.9458$ , through the ROC and DCA measurement models, it is verified that IPSRC performs better than SRC.

Table.3 The accuracies, sensitivity and specificity

Dataset			Information genes-10			
			SNMF[27]	ML-NMF[43]	ML-SNMF	LPML-SNMF
Breast-2	Accuracy (%)	IPSRC	77.14	84.94	87.94	<b><u>96.03</u></b>
		SRC	73.08	80.97	82.08	90.63
	Sensitivity (%)	IPSRC	77.5	84.50	87	<b><u>97.5</u></b>
		SRC	75	84.50	86.5	93
	Specificity (%)	IPSRC	76.67	85.83	89.17	<b><u>94.17</u></b>
		SRC	70	75.83	75.83	87.50

Table.4 The missed diagnosed and misdiagnose

Dataset			Information genes-10			
			SNMF[27]	ML-NMF[43]	ML-SNMF	LPML-SNMF
Breast-2	missed diagnosed	IPSRC	22.5	15.50	13	<b><u>2.5</u></b>
		SRC	25	15.50	13.5	7
	misdiagnosis	IPRC	23.33	14.17	10.83	<b><u>5.83</u></b>
		SRC	30	24.17	24.17	12.5

Table.5 The positive predictive value and positive predictive value

Dataset			Information genes-10			
			SNMF[27]	ML-NMF[43]	ML-SNMF	LPML-SNMF
Breast-2	positive predictive value	IPSRC	82.67	90.33	90.5	<b><u>95.83</u></b>
		SRC	79.5	84.83	84.83	93
	negative predictive value	IPSRC	72	75	86.67	<b><u>96.67</u></b>
		SRC	67.83	85	87	93

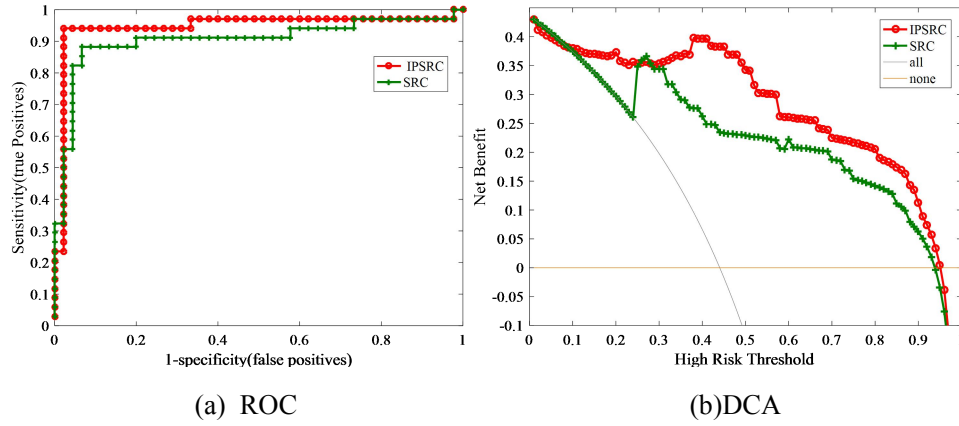


Fig.14 ROC analysis of IPSRC and SRC on Breast-2 database.

### 3.4.3 Comparison of different classification methods

In this section, the performance of IPSRC is compared with NN [52], SVM [28], CRC [31] and SRC [29]. Experiments were performed on a Breast-2 database, gene selection based DIF, feature selection based LPML-SNMF, and the resulting feature traits into different classifiers.

Table 6 shows the accuracies of different classifiers in the same environment. The selected feature of MLSNMF was based on IPSRC with the accuracy of 87.94%, which was 5.86% higher than the highest SRC82.08% of other classifiers. And the selected feature of LPML-SNMF was based on IPSRC with the accuracy of 96.03%, which was5.4% higher than the highest SRC 90.63% of other classifiers

Table.6 Different classification accuracies

Classifiers	Accuracy(%)		
	ML-NMF[43]	ML-SNMF	PML-SNMF
NN[52]	74.47	75.89	80.66
SVM[28]	78.12	78.61	84.62
CRC[31]	80.97	81.29	88.27
SRC[29]	80.97	82.08	90.63
IPSRC	<b>84.94</b>	<b>87.94</b>	<b>96.03</b>

Box plots of error rates are shown in Fig.15 after performing ten-fold cross validation. Fig.15 illustrates that NN, SVM, CRC, SRC, IPSRC achieve average error rates (red line) of 24.11%, 21.39%, 18.71%, 11.09% and 0 on Breast-2 database. Fig.15 represents that our method IPSRC the lowest error rate, the best classification.

And layer-wise pre-training ML-SNMF has the lowest error rate. Overall, a robust result with relatively low error rate can be offered by representation based methods. In other words, one can draw a conclusion that classification via IPSRC brings benefits to breast tumor classification in terms of error rate.

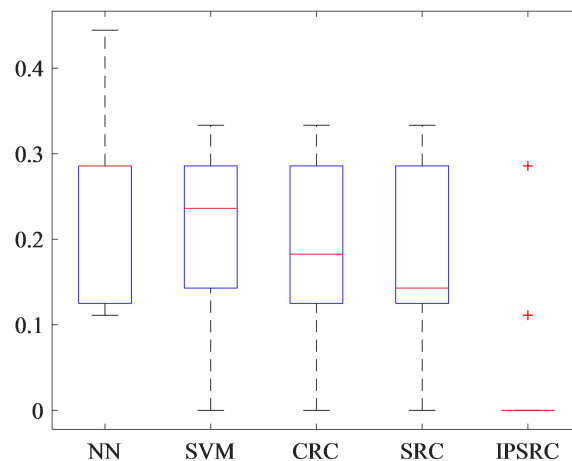


Fig.15 Box plots for error rates of three classifiers

ROC analysis of the ability of NN,SVM,CRC,SRC and IPSRC on Breast-2 dataset. Note that on the vertical axis, the scale is from no (0) to complete (1 or 100%) sensitivity. The horizontal axis is a reciprocal scale (1-specificity). The optimum performance of a test is determined either as the highest sum of the specificity and sensitivity or at an acceptable level of sensitivity for the given disease.

Fig.16 represent ROC analysis of the ability of NN, SVM, CRC, SRC, IPSRC. Table 7 is the AUC of the ROC for each classifier. Note that on the vertical axis, the scale is from no (0) to complete (1 or 100%) sensitivity. The horizontal axis is a reciprocal scale (1-specificity). The optimum performance of a test is determined either as the highest sum of the specificity and sensitivity or at an acceptable level of sensitivity for the given disease. Fig.16 (a) represent the features obtained by ML-SNMF are based on the classification results of different classifiers. Fig.16 (b) represent the features obtained by LPML-SNMF are based on the classification results of different classifiers. Table 9 and Fig.16 show that IPSRC achieves competitive results with highest AUC. The selected feature of ML-SNMF was based on IPSRC with the AUC of 0.8837, it was higher than the highest SVM 0.8805 of other classifiers. And LPML-SNMF, the AUC 0.9458 of IPSRC, it was higher than the highest SRC 0.9059 of other classifiers. Which show IPSRC has the best prediction

ability among the five classifiers. ROC plot analysis in Fig.16 have shown that IPSRC has the better discrimination ability than NN, SVM, CRC and SRC.

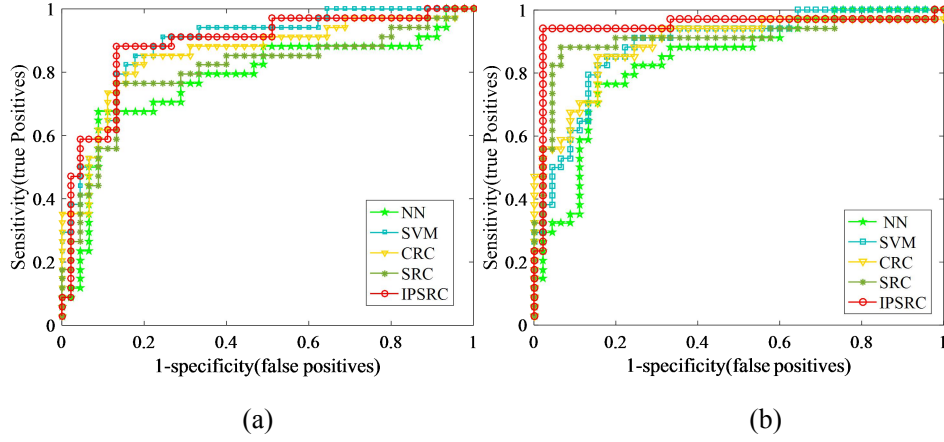


Fig.16 ROC analysis of the ability of NN, SVM, CRC, SRC and IPSRC on Breast-2 database.  
(a) The features obtained by ML-SNMF based on different classifiers, (b) The features obtained by LPML-SNMF based on different classifiers

Table. 7 AUC of different classifiers on Breast-2 database.

Classifiers	AUC	
	ML-SNMF	LPML-SNMF
NN	0.7778	0.8353
SVM	0.8805	0.8895
CRC	0.8569	0.8915
SRC	0.8026	0.9059
IPSRC	<b>0.8837</b>	<b>0.9458</b>

### 3.4.4 Comparing with state-of-the-art methods

Apart from based tumor classification methods and some popular classifiers, we also compare our method with some other in the latest articles in recent years. Table 8 and Table 9 prove that our algorithm is still competitive with higher accuracies than these articles. And we also compare our method with some other state-of-the-art methods, including PFSR [13],RRC\_L1 [32] and RRC\_L2 [32], which are also performed on Breast-2, Breast-2(97) and Breast-2(77) databases. Table 10 prove that our algorithm is still competitive with higher accuracies than these methods.

This part explores the classification results of breast tumors based on the Breast-2(97), Breast-2(77) database in recent years compared with the classification results of this article. Table 8 shows that on the Breast-2 (97) dataset, the latest articles



in recent years use 10-fold cross validation, the highest accuracy was 87.4%. Our method in the same dataset and same environment, the accuracy was 94%. 6.6% above the highest accuracy. Table 9 shows that on the Breast-2 (77) dataset, the latest articles in recent years the highest accuracy was 80.03%. Our method in the same dataset and same environment, the accuracy was 94.92%, 14.89% above the highest accuracy.

More intuitively, ERR is introduced to demonstrate that our method is superior to latest articles.

$$ERR = \frac{ER_1 - ER_2}{ER_1} \times 100\% ,$$

where  $ER_1$  is the error rate of the latest article classification result,  $ER_2$  is the error rate of our method classification result, ERR is denoted by a notion  $\downarrow$ . Table 12 shows that the error rate of this paper is 74.60% less than that of the latest Zhang et al. (2017), which is 74.21% lower than that of Fan et al. (2015). Table 11 and 12 show that our method classification performance is better than latest classification results. The results prove that our method is effective and practical.

Table.8 Classification accuracies based on different methods on Breast-2(97)

Methods	Accuracy(%)
Jiang et al.(2017) [25]	80
Su et al.(2017) [3]	87.4
<b>Our method</b>	<b>94</b>

Table.9 Classification accuracies based on different methods on Breast-2(77)

Methods	Error Rate (%)	ERR(%)
<b>Our method</b>	<b>5.08</b>	<b>-</b>
Zhang et al.(2017) [5]	20	$\downarrow$ 74.60
Fan et al.(2015) [4]	19.97	$\downarrow$ 74.21

RRC\_L1 and RRC\_L2 are the RRC coding model with L1 and L2 constraints respectively. Table 10 shows the results on Breast-2, Breast-2(97) and Breast-2(77) database in the same experimental setting. One can observe that our method achieves

competitive results of classification accuracies.

Table.10 Classification accuracies based on different methods onBreast-2, Breast-2(97) and Breast-2(77) database

Methods	Accuracy(%)		
	Breast-2	Brest-2(97)	Breast-2(77)
RRC_L1 [32]	89.38	84.31	85.12
RRC_L2 [32]	88.59	85.44	86.55
PFSRC [13]	88.27	84.32	85.44
<b>IPSRC</b>	<b>96.03</b>	<b>94</b>	<b>94.92</b>

### 3.5 Analysis of Candidate's Pathogenic Genes

#### 3.5.1 Analysis of information genes

Apart from obtaining high classification accuracy results, it is also important to identify pathogenicity-related genes, which can be a biomarker of early diagnosis and be helpful to auxiliary diagnosis. Pathogenicity-related genes selected in this article are information genes. Firstly, the basic biological attribute description of the information genes for classification is given, and then the specific biological description and rationality verification of some selected information genes are given. Analysis of genes in the Breast-2 database as an example.

Table.11 Decision-making information genes and their biological properties for classification on the Breast-2 dataset

Index no.of selected genes	Gene accession number	Gene description
NM_000286	PEX12	peroxisomal biogenesis factor 12
AL080059	TSPYL5	TSPY like 5
NM_014968	PITRM1	pitrilysinmetallopeptidase 1
AF052087	CACTIN	cactin, spliceosome C complex subunit
NM_003239	TGFB3	transforming growth factor beta 3
U45975	INPP5J	inositol polyphosphate-5-phosphatase J
NM_001685	ATP5J	ATP synthase, H <sup>+</sup> transporting, mitochondrial Fo complex subunit F6
NM_019028	ZDHHC13	zinc finger DHHC-type containing 13

Table 11 shows the basic biological attributes of the 10 information genes used for classification. Since there are two genes that do not contain the gene name and

description, only 8 genes were reanalyzed. In order to further test the validity of the selected genes, the expression profiles of the selected information genes in the Breast-2 data were next analyzed, the mean variance plot and scatter plot were used to give the four selected pathogenic genes and two unrelated genes compare results.

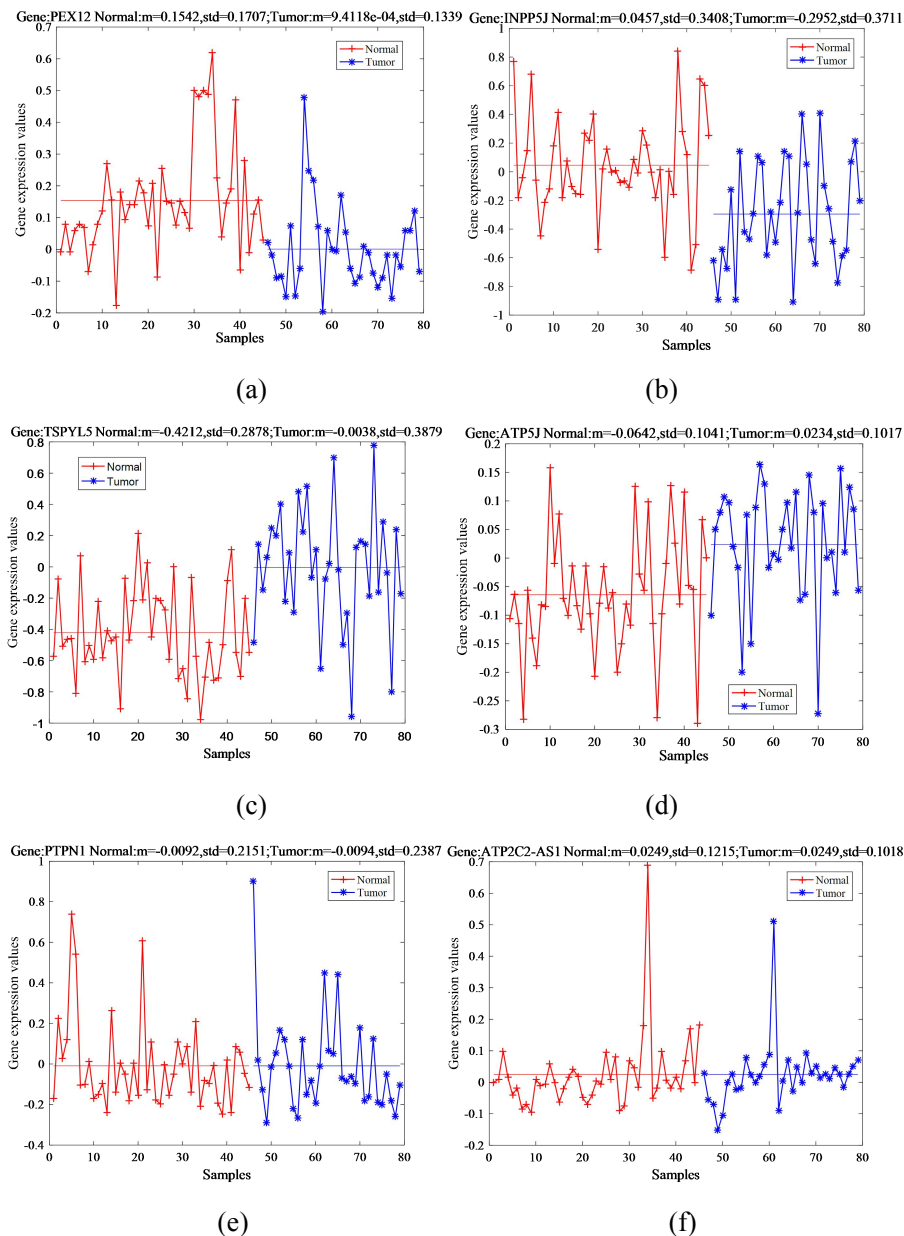


Fig.17 Comparison of expression levels for the pathogenic genes and irrelevant genes. The red and blue colors correspond to normal and tumor types respectively. (a, b, c, d) pathogenic genes (PEX12, INPP5J, TSPYL5 and ATP5J), and (e, f) PTPN1 and ATP2C2-AS1 are equally expressed for tumor and normal.

In order to check the quality of the selection processes, the expression profiles of the final identified genes for the opposite category are analyzed. For comparison, two irrelevant genes chosen randomly are presented. Fig.17 illustrates the two exemplary

expression levels of the patients for the pathogenic gene (PTPN1 and ATP2C2-AS1) listed in Table 14 and four irrelevant genes (PEX12, INPP5J, TSPYL5 and ATP5J). In Fig.17, the red line denotes gene expression levels of 45 normal samples and the blue line expresses gene expression levels of 34 tumor samples. The line indicates the mean values of gene expression levels in corresponding class. One can see in both cases the mean value of the samples belonging to breast tumor category differs significantly from the referenced (normal) category.

In the case of the pathogenic genes (Figs.17 (a), (b), (c) and (d)), the differences of the mean values are 0.1533, 0.3410, 0.4174 and 0.1683 respectively. For the irrelevant genes (Figs.17 (e) and (f)), the difference of the mean values in this case is 0. Moreover, one can see it fluctuates more greatly between binary-category than irrelevant genes by standard deviation (std).

Further more vividly illustrate the results of this article. Fig.18 shows the image of the expression profiles for the two pathogenic genes (TSPYL5 and ATP5J) and two irrelative genes (PTPN1 and ATP2C2-AS1) in the form of the heatmap of jet, where transition from blue to red colors corresponds to a shift from low to high expression values of the samples. The vertical axis represents samples (13 tumor samples, 10 normal samples). Fig.18 demonstrate that moderate to high up regulation of TSPYL5 and ATP5J and down regulation for other two genes can indicate the presence of Breast tumor distant metastases. There is a visible difference between samples of the Breast tumor group and the reference one in TSPYL5 and ATP5J but similar expression levels in PTPN1 and ATP2C2-AS1, which confirms good performance of the proposed gene selection procedure.

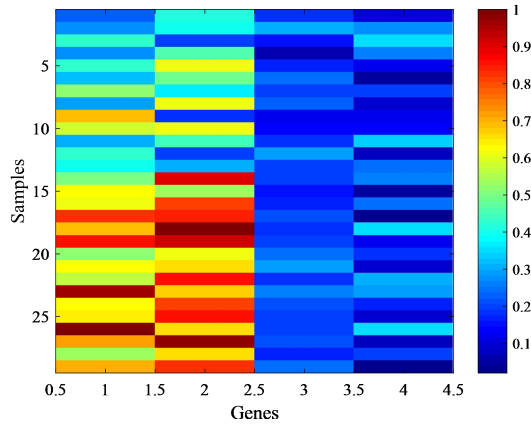


Fig.18 Pseudo color image of the samples for the Colon dataset. Each panel corresponds to one gene. Blue to red colors represents low to high expression levels of samples. The image reveals that moderate to high up regulation of TSPYL5 and ATP5J and down regulation for other two genes can signal Breast tumor.

For genes selected by our method DIF, we further do Kaplan-Meier curve by Anglicizing survival curves and corresponding Log-Rank p values on the website <http://www.oncolnc.org> and <http://ualcan.path.uab.edu/index.html>. From Fig.19, we can know that TSPYL5 ( $p=0.0362$ ) is anti-oncogene, PITRM1 ( $p=0.0066$ ) and ATP5J ( $p=0.0104$ ) are proto-oncogenes. For the two genes, high expression and low expression have significant difference in survival rate.

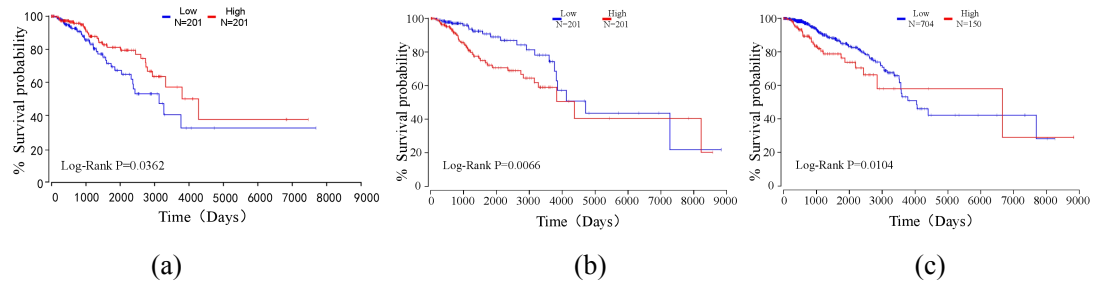


Fig.19 Kaplan-Meier survival curves of ( $p<0.05$ ). (a) TSPYL5; (b) PITRM1; (c) ATP5J

In order to further analyze the selected pathogenic genes, find out whether the specific biological functions of these genes in NCBI and related materials have biological significance for breast tumor. The specific biological information of several genes is given below. Some genes from the final candidate subset for Breast-2 data are shown in Table 11, which are believed to be closely related to Breast tumor. Gene TSPYL5 has been turned out to be associated with Breast tumor in clinical and some pathogenic genes also emerged in the study of others.

Gene TSPYL5 specific biological description: TSPYL5 knockdown decreased, and overexpression increased aromatase (CYP19A1) expression in MCF-7 cells, LCLs,

and adipocytes through the skin/adipose (I.4) promoter. TSPYL5 induced CYP19A1 expression and that of many other genes. In summary, genome-wide significant SNPs in TSPYL5 were associated with elevated plasma E2 in postmenopausal breast tumor patients [46].

Gene ATP5J specific biological description: Mitochondrial ATP synthase catalyzes ATP synthesis, utilizing an electrochemical gradient of protons across the inner membrane during oxidative phosphorylation. Alternatively spliced transcript variants encoding different isoforms have been identified for this gene.

PITRM1: The protein encoded by this gene is an ATP-dependent metalloprotease that degrades post-cleavage mitochondrial transit peptides. Genetic variation in the hPreP gene PITRM1 may potentially contribute to mitochondrial dysfunctions [49].

### **3.5.2 Gene enrichment analysis**

To further study the biological function of the candidate pathogenicity-related genes. We first selected 500 genes from the BW gene and selected the top 200 information genes for the selected 500 genes based on the DIF, of which 129 genes were found. We also perform the functional enrichment analysis of the top 200 genes identified by our method on the website <https://david.ncifcrf.gov/>. The results of KEEG\_PATHWAY are listed in Table 12. It can be seen from this table that the item of metabolic pathways has the lowest p-value, so it is considered as the most probable enrichment item. Only this pathway has statistical meaning ( $p < 0.05$ ). For genes enrich by our method, we further do Kaplan-Meier curve by Anglicizing survival curves and corresponding Log-Rank p values on the website <http://www.oncolnc.org> and <http://ualcan.path.uab.edu/index.html>. It can be seen from this Table.13 that there are 8 genes with statistical meaning ( $p < 0.05$ ), 7 are proto-oncogenes and 1 anti-oncogene. On Fig.20 we show the survival curve of 6 genes. From Fig.20, we can know that NME5( $p=0.0134$ ) is anti-oncogene, LPCAT1 ( $p=0.0183$ ), PGAM1 ( $p=0.0476$ ), UQCRC2( $p=0.0446$ ), GMPS( $p=0.0271$ ), CTPS1 ( $p=0.0462$ ) are proto-oncogenes. For the two genes, high expression and low expression have significant difference in survival rate.

Table.12 KEGG-PATHWAY terms enrichment analysis of the top 200 genes in the Breast-2 data set by DAVID

Rank	KEGG_PATHWAY	P-Value
1	Metabolic pathways	2.1e-2
2	Valine, leucine and isoleucine degradation	5.9e-2
3	Leukocyte trans endothelial migration	7.6e-2
4	Cell cycle	8.6e-2

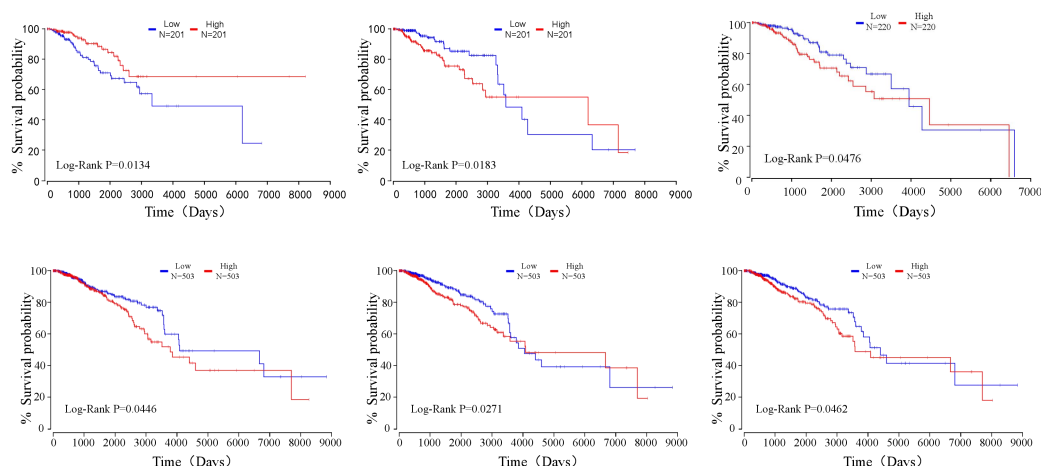


Fig.20.Kaplan-Meier survival curves of genes which enrich in pathways with statistical meaning( $p < 0.05$ ).Subimages from left to right:NME5,LPCAT1, PGAM1, UQCRC2, GMPS and CTPS1 respectively. Red lines denote upper percentile and blue lines denote lower percentile.

Table.13 Survival curves of statistical meaning ( $p < 0.05$ ) genes after functional enrichment analysis

Index no.of genes	Gene Name	Gene description	P-value
NM_003551	NME5-NME/NM23 family member 5	anti-oncogene	0.0134
AF_052162	LPCAT1-lysophosphatidylcholine acyltransferase 1	proto-oncogenes	0.0183
NM_002629	PGAM1-phosphoglycerate mutase 1	proto-oncogenes	0.0476
NM_003366	UQCRC2-ubiquinol-cytochrome c reductase core protein II	proto-oncogenes	0.0446
NM_003875	GMPS-guanine monophosphate synthase	proto-oncogenes	0.0271
NM_001905	CTPS1-CTP synthase 1	proto-oncogenes	0.0462
NM_001689	ATP5G3-ATP synthase, H <sup>+</sup> transporting, mitochondrial Fo complex subunit C3 (subunit 9)	proto-oncogenes	0.00011
NM_001685	ATP5J-ATP synthase, H <sup>+</sup> transporting, mitochondrial Fo complex subunit F6	proto-oncogenes	0.0056

The genes in Table.13 are considered to be associated with breast tumor. Gene PGAM1 has been turned out to be associated with breast tumor in clinical and some pathogenic genes also emerged in the study of others [48]. For further analysis, taking

PGAM1 and CTPS1 as examples, find out whether the specific biological functions of these genes in NCBI and related materials have biological significance for breast tumor.

**PGAM1:** Phosphoglycerate mutase 1 (PGAM1) is an important glycolytic enzyme that coordinates glycolysis. Knockdown of PGAM1 in tumor cells accelerates CtIP degradation through deprivation of the intracellular deoxyribonucleotide triphosphate pool and associated activation of the p53/p73 pathway. Enzymatic inhibition of PGAM1 decreases CtIP protein levels, impairs HR repair, and hence sensitizes BRCA1/2-proficient breast tumor to poly(ADP-ribose) polymerase (PARP) inhibitors.

**CTPS1:** This gene encodes an enzyme responsible for the catalytic conversion of UTP (uridine triphosphate) to CTP (cytidinetriphosphate). This reaction is an important step in the biosynthesis of phospholipids and nucleic acids. Activity of this protein is important in the immune system, and loss of function of this gene has been associated with immunodeficiency.

#### **4 Conclusions**

In this paper, a robust breast tumor recognition framework is presented based on considering reducing clinical misdiagnosis rate and exploiting available information in existing samples. A wrapper gene selection method DIF is established from a new perspective of reducing clinical misdiagnosis rate. The further feature selection of information genes is fulfilled by LPML-SNMF model, which is motivated by hierarchical learning and layer-wise pre-training strategy in deep learning. For completing the classification, the IPSR model is constructed to exploit information embedded in existing samples, especially in test ones. Moreover, the IPSR model is optimized via generalized ADMM and the corresponding convergence is analyzed. And verified that our robust breast tumor recognition framework is effective on three databases. Another is how to integrate feature learning and classification in a model framework

Furthermore, some valuable analysis and biological meanings of information genes are given. There remain some interesting questions. One is how to enforce some prior constraints into the IPRC model.



## Acknowledgements

The authors would like to thank <https://tumorgenome.nih.gov/> for their breast datasets. We also thank Prof. Yunhai Xiao provides their GADMM algorithm, Dr. Yue Li and Pei Wang for bioinformatics' suggestion, Chenxi Tian and Lei Sun for discussion. This work was supported in part by National Natural Science Foundation of China (11701144), Key Project of the Education Department Henan Province (14A120009), Natural Science Foundation of Henan Province (162300410061) and Project of Emerging Interdisciplinary (xxjc20170003). X.H. Yang is the corresponding author.

## References

- [1] Yuan Gao, P. George Church, "Improving molecular tumor class discovery through sparse non-negative matrix factorization," *ORIGINAL PAPER*, vol. 21, no. 21, pp. 3970–3975, 2005.
- [2] L. J. van't Veer, H. Dai, M. J. van de Vijver, et al., "Expression profiling predicts outcome in breast tumor," *Breast Tumor Research*, vol. 5, no. 1, pp. 57–58, 2003.
- [3] However, "A Cancer Gene Selection Algorithm Based on the K-S Test and CFS," *Biomed Research International*. 2017
- [4] Y Fan, Y kong, D Li, Z Zheng, "Innovated interaction screening for high-dimensional nonlinear classification," *Annals of Statistics*, vol. 43, no. 3, pp. 1243–1272, 2015.
- [5] D Zheng, J Jia, X Fang, X Guo, "Main and Interaction Effects Selection for Quadratic Discriminant Analysis via Penalized Linear Regression," arXiv:1702.0457v1. 2017.
- [6] Y. Bengio, "Learning deep architectures for ai," *Foundations and trends in Machine Learning*, vol. 2, no. 1, pp. 1–127, 2009.
- [7] R Rajabi, H Ghassemian, "Sparsity Constrained Graph Regularized NMF for Spectral Unmixing of Hyperspectral Data," *Journal of the Indian Society of Remote Sensing*, vol. 43, no. 2, pp. 269–278, 2015.
- [8] Nicolas Gillis, Francis Glineur, "Using underapproximations for sparse nonnegative matrix factorization," *Pattern Recognition*, vol. 43, no. 4, pp. 1676–1687, 2010.
- [9] Zuyuan Yang, Guoxu Zhou, Shengli Xie, et al., "Blind Spectral Unmixing Based on Sparse Nonnegative Matrix Factorization," *IEEE Transactions on Image Processing*, vol. 20, no. 4,

pp. 1112–1125, 2011.

- [10] RuicongZhi, Markus Flierl, QiuqiRuan, and W. BastiaanKleijn, “Graph-Preserving Sparse Nonnegative Matrix Factorization With Application to Facial Expression Recognition,” *IEEE Transactions on Systems Man & Cybernetics Part B Cybernetics A Publication of the IEEE Systems Man & Cybernetics Society*, vol. 41, no.1, pp. 38–52, 2011.
- [11] PO Hoyer, “Non-negative matrix factorization with sparseness constraints,” *Journal of Machine Learning Research*. Vol.5, no.1, pp.1457-1469, 2004.
- [12] A Nguyen, J Yosinski, J Clune, “Deep neural networks are easily fooled: High confidence predictions for unrecognizable images,” *Computer Vision and Pattern Recognition (CVPR)*, pp.427-436, 2015.
- [13] X. H. Yang, F. Liu, L. Tian, H. F. Li, X. Y. Jiang, “Pseudo-full-space representation based classification for robust face recognition,” *Signal Processing: Image Communications*, Vol.60 pp.64-78, 2018.
- [14] X. Hang and F.X. Wu, “Sparse representation for classification of tumors using gene expression data,” *Journal of Biomedicine & Biotechnology*. vol.2009, no.1, Article ID 403689, 2009.
- [15] C.H. Zheng, L. Zhang, T.Y. Ng, S.C. Shiu, and D.S. Huang, “Metasample-based sparse representation for tumor classification,” *IEEE/ACM Trans. Comput. Biol. Bioinformat.*, vol. 8, no. 5, pp. 1273-82, 2011.
- [16] B. Gan, C.H. Zheng, and J.X. Liu, “Metasample-Based Robust Sparse Representation for Tumor Classification,” *Engineering*, vol. 05, no. 5, pp. 78-83, 2013.
- [17] A Cichocki, R Zdunek, SI Amari, “Nonnegative matrix and tensor Factorization,” *IEEE Signal Processing Magazine*. vol. 25, no. 3, pp.54-65, 2008.
- [18] M.K. Khormuji and M. Bazrafkan, “A novel sparse coding algorithm for classification of tumors based on gene expression data,” *Med. Biol. Eng. Comput.* vol. 54, no. 6, pp. 869, 2016.
- [19] George Trigeorgis, Konstantinos Bousmalis, Stefanos Zafeiriou, Bjorn W. Schuller, “A Deep Matrix Factorization Method for Learning Attribute Representations,” *IEEE Transactions on Pattern Analysis & Machine Intelligence*, vol. 39, NO.3, pp. 417–429, 2017.
- [20] B. Gan, C.H. Zheng, J. Zhang, and H.Q. Wang, “Sparse representation for tumor classification based on feature extraction using latent low-rank representation,”

- Biomed.Res.Int*, vol. 2014, no. 10, pp. 63-68, 2014.
- [21] Blei, D. M. and Laerty, J. D. Topic models, Text mining: classification, clustering, and applications, vol. 10, no. 71, 34.
- [22] S Osher, Y Mao, B Dong, W Yin, "Linearized Bregman Iterations for Compressed Sensing," *Mathematics of Computation*, vol. 78, no. 268, pp. 2127-2136, 2009.
- [23] L. Zhang, M. Yang, and X. Feng, "Sparse representation or collaborative representation: which helps face recognition?" *IEEE International Conference on Computer Vision*, vol. 2011, no. 5, pp. 471-478, 2012.
- [24] ET Liu, C Sotiriou, "Defining the galaxy of gene expression in breast cancer," *Breast Cancer Research Bcr*, Vol. 4, no. 4, pp. 141-144, 2002.
- [25] B Jiang, Z Chen, C Leng, "Dynamic Linear Discriminant Analysis in High Dimensional Space," arXiv:1708.00205v2. 2017.
- [26] Daniel D. Lee, H. Sebastian Seung, "Learning the parts of objects by non-negative matrix factorization," *Nature*, vol. 401, no. 6755, pp. 788-791, 1999.
- [27] Hoyer P O, "Non-negative sparse coding," *IEEE Workshop on Neural Networks for Signal Processing*, vol. 0202009, no. 02, pp. 557-565, 2004.
- [28] T.S. Furey, N. Cristianini, N. Duffy, D.W. Bednarski, M. Schummer, and D. Haussler, "Support vector machines classification and validation of tumor tissue samples using microarray expression data," *Bioinformatics*, vol. 16, no. 10, pp. 906-914, 2000.
- [29] J. Wright, A.Y. Yang, A. Ganesh, S.S. Sastry, and Y. Ma, "Robust facerecognition via sparse representation," *IEEE Transactions on Pattern Analysis and Machine Intelligence*, vol. 31, no. 2, pp. 210-227, 2009.
- [30] Zhongyi Han, Benzhenh Wei, Yuanjie Zheng, Yilong Yin, Kejian Li, Shuo Li. Breast cancer multi-classification from histopathological images with structured deep learning, *Science Reports*, 2017, 7: 4172.
- [31] B. Gan, C. H. Zheng, J. Zhang, and H. Q. Wang, "Sparse representation for tumor classification based on feature extraction using latent low-rank representation," *Biomed Research International*, vol. 2014, no. 10, pp. 63-68, 2014.
- [32] M. Yang, L. Zhang, J. Yang, D. Zhang, "Regularized robust coding for face recognition," *IEEE Trans, Image Processing*, vol. 22, no. 5, pp. 1753-1766, 2013.

- [33]M. Welling, “Fisher linear discriminant analysis,” *Department of Computer Science*, vol. 16, no. 94, pp. 237-280, 2007.
- [34]L. Breiman, “Random forest,” *Machine Learning*, vol. 45, pp. 5-32, 2001.
- [35]D.P. Bertsekas, and J.N. Tsitsiklis, “Neural networks for pattern recognition,” *Agricultural Engineering International the Cigr Journal of Scientific Research & Development Manuscript Pm*, vol. 12, no. 5, pp. 1235 – 1242, 1995.
- [36] Y. Bengio, A. Courville, P. Vincent. Representation learning: a review and new perspectives. *IEEE Transactions on Pattern Analysis and Machine Intelligence*. 2012, 35(8): 1798-828..
- [37] CH Zheng, TY Ng, L Zhang, CK Shiu, HQ Wang, Tumor Classification Based on Non-Negative Matrix Factorization Using Gene Expression Data, *IEEE Transactions on Nanobioscience*. 2011 , 10 (2) :86-93
- [38] X. Chen, Y. Zhao, Y.Q. Zhang, and R. Harrison, “Combining SVM classifiers using genetic fuzzy systems based on AUC for gene expression data analysis,” *Proc. Bioinformat, Res. Appl.*, vol. 4463, pp. 496-505, 2007.
- [39] J Xie, M Wang, HU Qiufeng, “The differentially expressed gene selection algorithms for unbalanced gene datasets by maximize the area under ROC”, *Journal of Shaanxi Normal University*, 2017.
- [40] MR Hestenes, “Multiplier and gradient methods,”*Journal of Optimization Theory & Applications*,vol. 4, no. 5, pp. 303-320, 1969.
- [41] Y Xiao, L Chen, D Li, “A Generalized Alternating Direction Method of Multipliers with Semi-Proximal Terms for Convex Composite Conic Programming,”*Mathematical Programming Computation*, pp. 1-23, 2018.
- [42]A. Cichocki, R. Zdunek, “Multilayer Nonnegative Matrix Factorization,”*Electronics Letters*, vol. 42, no. 16, pp. 947-948, 2006.
- [43] A. Cichocki, R. Zdunek.Multilayer Nonnegative Matrix Factorization Using Projected Gradient Approaches,”*International Journal of Neural Systems*,vol. 17, no. 6, pp. 431–446, 2007.
- [44] B Efron, T Hastie, I Johnstone, “Least angle regression,”*Annals of Statistics*, vol. 32, no. 2, pp. 407-451, 2002.
- [45] Andrew J. Vickers, Elena B. Elkin,“Decision curve analysis: a novel method for evaluating

- prediction models,” *NIH-PA Author Manuscript*, vol. 26, no.6, pp. 565–574, 2006.
- [46] AP Bradley, “The use of the area under the ROC curve in the evaluation of machine learning algorithms,” *Pattern Recognition*, vol. 30, no. 7, pp. 1145-1159, 1997.
- [47] B Weigelt, HM Horlings, B Kreike, MM Hayes, “Refinement of breast tumor classification by molecular characterization of histological special types,” *Journal of Pathology*, vol. 216, no. 2, pp. 141-150, 2008.
- [48] Qu J, Sun W, Zhong J, Lv H et al., “Phosphoglycerate mutase 1 regulates dNTP pool and promotes homologous recombination repair in tumor cells,” *Journal of Cell Biology*, vol. 216, no. 2, pp. 409-424, 2017.
- [49] Pinho CM, Björk BF, Alikhani N et al., “Genetic and biochemical studies of SNPs of the mitochondrial A beta-degrading protease,” *Neuroscience Letters*, 2010; vol. 469, no. 2, pp.204-208, 2010.
- [50] S. Dudoit, J. Fridlyand, and T.P. Speed, “Comparison of discrimination methods for the classification of tumors using gene expression data,” *Journal of the American Statistical Association*, vol. 97, no. 457, pp. 77-87, 2002.
- [51] T.R. Golub, D.K. Slonim, P. Tamayo, C. Huard, M. Gaasenbeek, J.P. Mesirov, H. Coller, M.L. Loh, J.R. Downing, M.A. Caligiuri, C.D. Bloomfield, and E.S. Lander, “Molecular classification of tumor: class discovery and class prediction by gene expression monitoring,” *Science*, vol. 286, no. 5439, pp. 531-537, 1999.
- [52] Cover T W, Hart P E, “Nearest Neighbor Pattern Classification,” *IEEE Trans On Information Theory*, vol. 13, no. 1, pp. 21-27, 1967.
- [53] R. Tibshirani, “Regression shrinkage and selection via the Lasso,” *Journal of the Royal Statistical Society. Series B*, vol. 58, no. 1, pp. 267-288, 1996.
- [54] XiaoBo Zhou, XiaoDong Wang, Edward R. Dougherty, “Nonlinear probit gene classification using mutual information and wavelet-based feature selection,” *Journal of Biological Systems*, vol. 12, no. 3, pp. 371-386, 2004.
- [55] C Sotiriou, SY Neo, LM Mcshane, EL Korn, PM Long, “Breast cancer classification and prognosis based on gene expression profiles from a population-based study,” *Proceedings of the National Academy of Sciences of the United States of America*, vol. 100, no. 18, pp.10393-10398, 2003.

- [56] LJ van, H Dai, MJ van, YD He, "Gene expression profiling predicts clinical outcome of breast cancer," *Nature*, vol. 415, no. 6871, pp. 530-536, 2002.
- [57] Y Chen, Z Zhang, J Zhen, Y Yue, "Gene selection for tumor classification using neighborhood rough sets and entropy measures," *Journal of Biomedical Informatics*, vol. 67 pp. 59-68, 2017.
- [58] Y Li, N Alioune, "The non-negative matrix factorization toolbox for biological data mining," *Source Code for Biology & Medicine*, vol.8, no. 1, 2013.
- [59] ZY Algamal, HTM Ali, "An efficient gene selection method for high-dimensional microarray data based on sparse logistic regression," *Electronic Journal of Applied Statistical Analysis*, vol. 10, no.1, pp. 242-256, 2017.
- [60] M Dashtban, M Balafar, "Gene selection for microarray cancer classification using a new evolutionary method employing artificial intelligence concepts," *Genomics*, vol. 109, no. 2, pp. 91-107, 2017.
- [61] E Benetos, M Kotti, C Kotropoulos, "Musical Instrument Classification using Non-Negative Matrix Factorization Algorithms and Subset Feature Selection," *IEEE International Conference on Acoustics Speech & Signal Processing*, vol. 5, no.1, pp. 221-224, 2006.
- [62] MD Gupta, "Non-negative matrix factorization as a feature selection tool for maximum margin classifiers," *IEEE Conference on Computer Vision & Pattern Recognition*, vol. 32, no. 14, pp. 2841-2848, 2011.